

1 **The impacts of fireworks burning at Chinese Spring Festival on air quality: insights of**
2 **tracers, source evolution and aging processes**

3 Shaofei Kong ^{1,2}, Li Li ², Xuxu Li ², Yan Yin ^{1,2*}, Kui Chen ^{1,2}, Dantong Liu ⁴, Liang Yuan ²,
4 Yingjie Zhang ², Yunpeng Shan ², Yaqin Ji ^{3*}

5 *1. Collaborative Innovation Center on Forecast and Evaluation of Meteorological*

6 *Disasters, Nanjing University of Information Science and Technology, Nanjing, 210044, China*

7 *2. Key Laboratory for Aerosol-Cloud-Precipitation of China Meteorological Administration, School of*
8 *Atmospheric Physics, Nanjing University of Information Science & Technology, Nanjing 210044, China*

9 *3. Colloge of Environemental Science and Engineering, Nankai University, Tianjin, 100086, China*

10 *4. School of Earth, Atmospheric and Environmental Science, University of Manchester, Manchester, UK*

11 **Abstract:**

12 To understand the impact of fireworks burning (FW) particles on air quality and human
13 health during winter haze period, thirty-nine elements, ten water-soluble ions and eight fractions
14 of carbonaceous species in atmospheric PM_{2.5} at Nanjing were investigated during 2014 Chinese
15 Spring Festival (SF). Serious regional haze pollution persisted throughout the entire sampling
16 period, PM_{2.5} averaging at 113±69 μg m⁻³ and visibility at 4.8±3.2 km. The holiday effect led to
17 almost all the chemical species decreasing during the SF, except for Al, K, Ba and Sr which were
18 related to FW. The source contributions of coal combustion, vehicle emission and road dust
19 decreased dramatically, whereas FW contributed to about half of the PM_{2.5} during SF period. The
20 intensive emission of FW particles at New Year's Eve accounted for 60.1% of the PM_{2.5}. They
21 also **obviously** modified the chemical compositions of PM_{2.5}, with 39.3% contributed by increased
22 organic matter, followed by steadily increased loadings of secondary inorganic ions. The aging
23 processes of the FW particles **lasted for about four days reflected by the variations of Ba, Sr, NH₄⁺,**
24 **NO₃⁻, SO₄²⁻ and K⁺**, characterized by heterogeneous reactions of SO₂ and NO_x on crustal materials
25 directly from FW, the replacement of Cl⁻ by NO₃⁻ and SO₄²⁻, coating of NO₃⁻ and SO₄²⁻ on soot,
26 formation of secondary organic aerosols and metal-catalyzed formation of NO₃⁻ and SO₄²⁻ at
27 higher relative humidity. During aging, the main contributors to the extinction coefficient shifted
28 from elemental carbon and organic matter to ammonium sulfate. The particles raised higher cancer
29 risks by heavy metals (especially for Cd and As) as 1.62×10⁻⁶. This study provided detailed
30 composition data and first comprehensive analysis of the aging processes of FW particles at

31 serious haze pollution period and their potential impact on human health.

32 **Keywords:** PM_{2.5}; chemical compositions; haze; fireworks burning particles; aging; health risk

33

34 * *Correspondence to:* Y. Yin (yinyan@nuist.edu.cn); Y.Q. Ji (jiyaqin@nankai.edu.cn); S.F. Kong
35 (kongshaofei@126.com)

36 Address: Nanjing University of Information Science and Technology, Ningliu Road 219, Nanjing,
37 China; Tel/Fax: +86-25-58731207

38

39 **Abbreviations glossary:**

40 Fireworks burning-FW

41 Chinese New Year day-CNY

42 Spring Festival-SF

43 Lantern Festival-LF

44 Organic carbon-OC

45 Elemental carbon-EC

46 Black carbon-BC

47 Organic matter-OM

48 Relative humidity-RH

49 Inductively coupled plasma-mass spectroscopy-ICP-MS

50 Inductively coupled plasma-optical emission spectrometer-ICP-OES

51 Optically detected pyrolyzed carbon-OPC

52 Principal component analysis-PCA

53 Lifetime average daily dose-LADD

54 Inhalation rate-InhR

55 Exposure frequency-EF

56 Exposure duration-ED

57 Average body weight-BW

58 **Averaging time-AT**

59 Hazard Quotient-HQ

60 Reference dose-RfD

61 Hazard Index-HI

62 Mineral matter-MIN

63 Trace elements-TE

64 Sea salt-SS

65 Secondary inorganic aerosol-SIA

66 Unidentified matter-UM

67 Correlation coefficient-R²

68 Weather Research and Forecast model-WRF

69 The day before CNY-Pre-CNY

70 The day before LF-Pre-LF

71 The period before Spring Festival-Pre-SF
72 The period after Spring Festival-After-SF
73 Mass calculated by adding individual components- PM_{cal}
74 Gravimetrically measured particulate mass- PM_{meas}
75 Visibility calculated by adding individual components- V_{cal}
76 Measured visibility- V_{meas}
77 Extinction coefficient- b_{ext}

78

79 **1 Introduction**

80 Atmospheric pollutants emitted from fireworks burning (FW) at festivals or special
81 celebration events around the world have recently received wide attention, such as Guy Fawkes'
82 night at UK (Allan et al., 2010; Godri et al., 2010), Pyronale® 2009 and Pyromusikale®
83 (Dutschke et al., 2011), Montréal International Fireworks competition (Joly et al., 2010), New
84 Year's celebrations (Williams et al., 2005; Drewnick et al., 2006; Zhang et al., 2010; Do et al.,
85 2012; Feng et al., 2012; Jiang et al., 2014; Jing et al., 2014; Tian et al., 2014; Ye et al., 2014),
86 Diwali (Godri et al., 2010), Las Fallas in Valencia (Moreno et al., 2007), new Millennium in
87 Germany (Wehner et al., 2000), 2006 FIFA World Cup (Vecchi et al., 2008) and Lantern Festival
88 (Do et al., 2012; Tsai et al., 2012). Besides the direct possible dangers like the exposure to sound
89 pressures (Dutschke et al., 2011) or firework-related injuries (Do et al., 2012), their burning results
90 in massive quantities of pollutants, leading to degradation of air quality (Wang et al., 2007; Sarkar
91 et al., 2010; Dutschke et al., 2011; Do et al., 2012; Feng et al., 2012; Tsai et al., 2012; Jiang et al.,
92 2014; Jing et al., 2014; Tian et al., 2014; Yang et al., 2014) and raising serious human health
93 concerns (Godri et al., 2010; Do et al., 2012). Evidence suggests that inhalation of fumes
94 containing high levels of specific elements such as chlorine can cause mucosal irritation and acute
95 respiratory distress syndrome (Joly et al., 2010). A toxicity study reported that the samples
96 collected in the post-FW period were more toxic than those in the pre-FW period according to the
97 viabilities of BEAS-2B cells after 24-h incubation with the particle extracts (Do et al., 2012). A
98 positive significant relationship was also found between particulate matter oxidative burden and
99 individual trace metals associated with FW (Godri et al., 2010).

100 China is the largest firework producing country in the world (Tian et al., 2014). For the
101 Chinese New Year day (CNY, in the Spring Festival (SF) at Jan. or Feb. of lunar Chinese calendar,
102 high-profile FW events occurred at the midnight of the CNY's Eve in national scale, from small

103 villages to megacities. It should be noted that FW events always occurred in an already highly
104 polluted urban air in China ([Supplementary file S1](#)). In winter, increased coal consumption for
105 heating ([Li and Zhang, 2014](#)) and stable atmospheric conditions always raise serious haze
106 pollution in central and eastern China. On January 2013, the whole central and eastern China was
107 shrouded in a long-lasting severe haze episode ([Wang et al., 2014](#)). According to the Chinese
108 Ministry of Environmental Protection, at Jan. 31, 2014, about 80% of 161 cities held average
109 PM_{2.5} concentrations higher than 150 µg m⁻³ ([Ye et al., 2014](#)). The addition of pollutants from FW
110 deteriorates ambient air quality during the SF and its impact can vary significantly with FW
111 duration and meteorological conditions ([Vecchi et al., 2008](#); [Yu et al., 2013](#)).

112 Previous studies have extensively characterized the physicochemical signatures of FW
113 emissions, such as gaseous pollutants ([Wehner et al., 2000](#); [Attri et al., 2001](#); [Williams et al., 2005](#);
114 [Drewnick et al., 2006](#); [Wang et al., 2007](#); [Vecchi et al., 2008](#); [Tan et al., 2009](#); [Godri et al., 2010](#)),
115 particle size distribution and number concentration ([Wehner et al., 2000](#); [Drewnick et al., 2006](#);
116 [Vecchi et al., 2008](#); [Zhang et al., 2010](#); [Dutschke et al., 2011](#); [Yang et al., 2014](#)), chemical
117 components including trace elements ([Wang et al., 2007](#); [Moreno et al., 2007](#); [Vecchi et al., 2008](#);
118 [Estrellan and Iino, 2010](#); [Godri et al., 2010](#); [Joly et al., 2010](#); [Do et al., 2012](#); [Tsai et al., 2012](#);
119 [Tian et al., 2014](#); [Yang et al., 2014](#)), organic carbon (OC) and elemental carbon (EC) ([Estrellan
120 and Iino, 2010](#); [Feng et al., 2012](#); [Tsai et al., 2012](#); [Tian et al., 2014](#); [Yang et al., 2014](#)) and
121 water-soluble ions ([Wang et al., 2007](#); [Vecchi et al., 2008](#); [Shen et al., 2009](#); [Estrellan and Iino,
122 2010](#); [Tsai et al., 2012](#); [Wang et al., 2013](#); [Jiang et al., 2014](#); [Tian et al., 2014](#); [Yang et al., 2014](#)).
123 Recently, single particle's chemical compositions ([Drewnick et al., 2006](#); [Allan et al., 2010](#); [Jiang
124 et al., 2014](#)), morphology and mixing properties ([Li et al., 2013](#)) and optical properties ([Yu et al.,
125 2013](#)) of FW particles had been reported. However, there are to date still two shortages.

126 Firstly, no studies reported the chemical compositions (crustal elements, trace elements,
127 water-soluble ions, OC and EC) of FW particles completely, considering the complex manufacture
128 materials of FW ([Supplementary file S2](#)). Although [Estrellan and Iino \(2010\)](#), [Feng et al. \(2012\)](#),
129 [Yang et al. \(2014\)](#) and [Tian et al. \(2014\)](#) reported the ions, elements and carbonaceous species
130 synchronously, some important species were missed, such as Na, Mg, K, Ti, NH₄⁺ and Cl⁻ in [Tian
131 et al. \(2014\)](#), OC in [Estrellan and Iino \(2010\)](#), Si and some heavy elements in [Feng et al. \(2012\)](#)
132 and crustal elements in [Yang et al. \(2014\)](#). These species are all highly elevated during FW events.

133 Crustal elements including Na, Mg, Al, Si, K, Ca, Ti, Fe and Mn were always missing or not
134 sufficiently studied in FW particles. However, except for inorganic and organic chemicals such as
135 charcoal, potassium nitrate, potassium chlorate, potassium perchlorate, sulfur, manganese, sodium
136 oxalate, aluminum, iron powder, strontium nitrate, and barium nitrate (Shen et al., 2009; Jing et al.,
137 2014), clay is also used to seal the top and bottom of fireworks as shown in Supplementary file S3.
138 90% of the total mineral aerosol was from the emission of FW on the lantern night in Beijing
139 (Wang et al., 2007). The incomplete compositions of FW particles may bias the identification of
140 particle sources during FW period and limit our understanding of its aging processes. For example,
141 crustal elements-Al, Si and Ca were thought to result from the resuspension of materials already
142 deposited on the ground (caused by pyrotechnic device explosions) and hereby the resuspended
143 dust was regarded as a contributor to atmospheric particles during SF (Tian et al., 2014). Without
144 detecting the crustal and trace elements, secondary particulate matter accounted for 63-82% of
145 PM_{1.0} during FW periods in Beijing (Jiang et al., 2014).

146 Secondly, all the former studies unanimously agreed with that FW contributed to elevated
147 concentrations of particles and associated chemical species, but no studies concerned the aging
148 processes of particles after emitted from intensive FW. The cocktail of primary pollutants released
149 may exhibit varied interactions among themselves, and if aided by favourable atmospheric
150 conditions, may lead to the formation of secondary pollutants (Sarkar et al., 2010). Do et al. (2012)
151 pointed that the sub-micron aerosol or accumulation-mode particles from FW can suspend in the
152 air for very long periods, from days to weeks, potentially causing pollution to large areas. Data in
153 literature verified the existence of aging processes of FW particles, though it has not been
154 discussed. For example, Li et al. (2013) indicated that emissions from FW changed the
155 transformation pathway from SO₂ to SO₄²⁻ and the FW particles can influence the air at downwind
156 site (50 km far away). And after about two days, the elevated PM_{2.5} mass concentrations at CNY's
157 Eve decreased to the level of the day before CNY (pre-CNY). In Beijing, PM_{2.5} mass
158 concentrations at CNY's Eve decreased to the level of pre-CNY in one day, while secondary ions
159 (SO₄²⁻, NH₄⁺ and NO₃⁻) and organic matter (OM) increased first and then decreased to the level of
160 pre-CNY after three days (Wang et al., 2007). In Jinan, a "tailing" phenomena was found,
161 indicating that NH₄⁺ and NO₃⁻ did not increase (peaking at 8:00 and 12:00, respectively)
162 immediately with the concentrations of particles (peaking at 00:00) after emitted at CNY's Eve

163 (Yang et al., 2014). In Shanghai, NH_4^+ and NO_3^- also increased in the first day after emitted at
164 CNY's Eve and then decreased to the level of pre-CNY in the third day and the decreasing rate of
165 $\text{PM}_{2.5}$ was faster than that for OC (Feng et al., 2012). Therefore, we still need to answer the
166 following questions: (1) are the decreasing trends of particles and associated chemical components
167 the same? (2) how long and how far can FW influence the air quality at certain meteorological
168 conditions? (3) during aging and transport, which type of chemical reactions will the FW particles
169 undergo and how will specific chemical ratios vary?

170 Due to rapid economic expansion and urbanization, the occurrence frequency of haze has
171 increased rapidly in recent 30 years at the Yangtze River Delta region (Wang et al., 2014). As one
172 of the central megacities of this region, Nanjing is suffering from serious air pollution and the
173 occurrence of hazy days increased from 1961 to 2005 (Kang et al., 2013). Thus, it provides an
174 unique site and opportunity to study the chemical composition evolution and source variation
175 during haze-clear days with the injection of intensive FW at SF. The main purposes of this study
176 are to: (1) characterize in detail the chemical compositions of atmospheric $\text{PM}_{2.5}$ before, during
177 and after intensive FW events; (2) identify how long and how much can the FW particles
178 influence $\text{PM}_{2.5}$ by tracer analysis and receptor models; (3) emphasize how can the FW particles
179 affect visibility and human cancer and non-cancer risks; (4) analyze the FW particle aging
180 processes by specific species and ratios. The data and analysis will improve the knowledge of
181 chemical compositions of FW particles, their evolution during serious haze pollution periods and
182 their influence on visibility and human health.

183 **2 Methodology**

184 **2.1 $\text{PM}_{2.5}$ collection**

185 From 24 Jan. to 21 Feb. 2014, a sampling campaign of $\text{PM}_{2.5}$ was conducted on the rooftop
186 (40 m high) of a building in Nanjing University of Information Science & Technology (Kang et al.,
187 2013; Wang et al., 2014). It is a suburban site, surrounded by residential communities at the west,
188 south, north and southeast directions. There is a steel factory 2 km to the east of the campus and a
189 chemical industry park about 10 km to the northeast. It faced one road with heavy traffic, about
190 200 m in the east. Location of the sampling site was shown in Fig.1 and Supplementary file S4.
191 During the sampling period, CNY at Jan. 30 and Lantern Festival (LF) at Feb.14 were included. In
192 CNY's and LF's Eve, numerous fireworks were consumed. The SF holiday was from Jan. 30 to

193 Feb.7. Each day, PM_{2.5} samples were collected at about 08:00 am for 24 h using two
194 medium-volume air samplers (TH-150C, Wuhan Tianhong Ltd., China) on quartz fiber filters
195 (baked at 800 °C for 2 h) and polypropylene fiber filters (baked at 80 °C for 0.5 h) at a flow rate of
196 100 L min⁻¹. The hourly online PM_{2.5} mass concentrations for the nine monitoring sites set by
197 Jiangsu Environmental Monitoring Center were collected from the public platform
198 (<http://218.94.78.75/jsair/>) (their locations can be found in [Supplementary file S4](#)). Twenty-four
199 pairs of filter samples were obtained ([Supplementary file S5](#)). By using a microbalance (Ohaus
200 Discovery DV214CD) with balance sensitivity as ±0.010 mg, filters were weighed before and
201 after sampling under controlled environment with temperature and relative humidity (RH) of
202 22 °C and 35%. Then they were stored at -20 °C until chemical analysis. The quartz fiber filters
203 were for analyzing water-soluble inorganic ions, OC and EC. Polypropylene fiber filters were for
204 elemental analysis.

205

(Fig.1)

206

208 2.2 Chemical analysis

209 Inductively coupled plasma-mass spectroscopy (ICP-MS) (Agilent 7500a, Agilent Co. USA)
210 was used for analyzing Li, Be, Na, Mg, Al, P, K, Ca, Sb, Sc, Ti, V, Cr, Mn, Co, Ni, Cu, Zn, As, Rb,
211 Y, Mo, Cd, Sn, Cs, La, Ce, Sm, W, Tl, Pb, Bi, Th and U. Nine elements including Si, Al, Ca, Mg,
212 Fe, Ti, Ba, Sr and Zr were analyzed by inductively coupled plasma-optical emission spectrometer
213 (ICP-OES). Al, Ca, Mg and Ti were analyzed by both ICP-MS and ICP-OES, and results from the
214 latter were used as the analysis accuracy for the four elements by ICP-OES was better than that by
215 ICP-MS ([Kong et al., 2014a](#)). Ten ions including NH₄⁺, Na⁺, Mg²⁺, K⁺, Ca²⁺, F⁻, Cl⁻, NO₂⁻, NO₃⁻
216 and SO₄²⁻ were analyzed by a professional Ion Chromatograph (Wan Tong 850, Switzerland). DRI
217 Model 2001 (Thermal/Optical Carbon Analyzer) with the IMPROVE thermal/optical reflectance
218 protocol was used for OC and EC analysis ([Han et al., 2008](#); [Han et al., 2010](#); [Huang et al., 2012](#);
219 [Li et al., 2012](#); [Wang et al., 2013](#); [Kong et al., 2014a](#)). A 0.188 cm² punch area from the quartz
220 filter was heated to produce four OC fractions: OC1, OC2, OC3 and OC4 at temperatures of 120,
221 250, 450 and 550°C in a non-oxidizing He atmosphere, three EC fractions: EC1, EC2 and EC3 at
222 550, 700 and 800°C in an oxidizing atmosphere of 2% O₂/98% He and optically detected

223 pyrolyzed carbon (OPC). OC is defined as OC1+OC2+OC3+OC4+OPC and EC is calculated by
224 EC1+EC2+EC3-OPC. Char-EC is defined as EC1 minus OPC, and soot-EC is the sum of EC2 and
225 EC3 (Han et al., 2008; Han et al., 2010). The pre-treatment and chemical analysis procedures and
226 quality assurance and control are described detailedly in our previous works (Li et al., 2012; Kong
227 et al., 2014a; 2014b; Li et al., 2014).

228 **2.3 Meteorological parameters**

229 The meteorological parameters including relative humidity (RH), visibility, wind speed, wind
230 direction and temperature were recorded by the meteorological observatory of our university
231 (<http://qxt.nuist.edu.cn/>). The rainfall information was obtained from
232 <http://www.wunderground.com/>. According to China Meteorological Administration, fog is defined
233 as visibility <10 km and RH>90% and haze is defined as visibility <10 km and RH<80%. For
234 visibility <10 km and 80%<RH<90%, it is fog-haze mixing day. Fig.2 shows that the visibilities
235 are generally below 10 km (averaged as 4.8 ± 3.2 km), indicating fog, haze or fog-haze mixing
236 events frequently occurred. At Feb.4, a strong cold front passed through, leading to high visibility
237 (14.7 km), low temperature (2.4°C) and high wind speed (3.5 m s^{-1}). The wind speed remained
238 mostly below 3 m s^{-1} (averaged as $2.2 \pm 0.7 \text{ m s}^{-1}$), suggesting stagnant weather conditions.

239

240 (Fig.2)

241

242 **2.4 Data processing**

243 **2.4.1 Back trajectory calculation**

244 Three-day air mass back trajectories are calculated using NOAA Air Resource Lab HYSPLIT
245 4.8 model, driven by the GDAS meteorological dataset ($1^\circ \times 1^\circ$) (Kong et al., 2014b). A 72 h back
246 trajectory is adopted with the starting height of 500 m above ground level (Huang et al., 2012).
247 Cluster analysis is adopted which results in sub-sets of trajectories with backward trajectories
248 computed every six hour (00:00, 06:00, 12:00 and 18:00) each day. The clustering process is
249 described in detail in Hysplit User' s Guide-Version 4. The mixing layer height is calculated every
250 three hours each day by the NOAA's READY Archived Meteorology online calculating program
251 (<http://ready.arl.noaa.gov/READYamet.php>). This program will produce a time-series of
252 calculated boundary layer depth using the chosen meteorological data. As shown in Fig.3, 43%

253 (cluster 3, 4 and 5) of the air masses originated from the Mongolia and crossed Chinese coastal seas;
254 31% (cluster 1) was from the north China and transported across Shandong peninsula; 26%
255 (cluster 2) was from central China. Cluster 1 and cluster 2 transported for short distances, which
256 may easily raise regional air pollution, as the Shandong peninsula and central and eastern China
257 hold intensive anthropologic sources for air pollutants.

258

259 (Fig.3)

260

261 2.4.2 Principal component analysis

262 Principal component analysis (PCA) is used to identify the sources for particles at periods
263 before (Jan. 24-29), during (Jan. 30-Feb. 6), after SF holiday (Feb. 12-Feb. 21) and the whole
264 period. It can analyze multivariate data sets structure and identify a smaller number of independent
265 factors to explain the data variance. Factor loadings are related to the source emission
266 compositions. A varimax normalized rotation is adopted by SPSS 13.0 software in this study
267 (Kong et al., 2010).

268 2.4.3 Health risk assessment of heavy metals

269 After emitted, the heavy metals in FW particles can raise risks to human health. To raise the
270 attention of public on the healthy threat of FW particles, the average amount of heavy metal
271 exposure by inhalation (D_{inh}) per an individual's body weight over a given time span for adult and
272 children was calculated by following equation (Kong et al., 2012; Yang et al., 2014):

$$273 \quad D_{inh} (mg \cdot kg^{-1} \cdot day^{-1}) = \frac{C \times InhR \times EF \times ED}{BW \times AT} \quad (1)$$

274 The lifetime average daily dose (LADD) of Co, Ni, As and Cd exposure through inhalation
275 was used for assessing cancer risk as following:

$$276 \quad LADD = \frac{C \times EF}{AT} \times \left(\frac{InhR_{child} \times ED_{child}}{BW_{child}} + \frac{InhR_{adult} \times ED_{adult}}{BW_{adult}} \right) \quad (2)$$

277

278 where C is exposure-point concentration. Its upper limit of the 95% confidence interval for
279 the mean is calculated as:

280
$$C_{95\%UCL} = \exp\left(\bar{X} + 0.5s^2 + \frac{s \times H}{\sqrt{n-1}}\right) \quad (3)$$

281 where \bar{X} is the arithmetic mean of the log-transformed data, s is the standard deviation of the
 282 log-transformed data, H is the H-statistic and n is the number of samples. InhR: inhalation rate, 7.6
 283 and 20 m³ day⁻¹ for children and adult; EF: exposure frequency, 4 day year⁻¹ in this study
 284 (according to the discussion in Section 3.4.2); ED: exposure duration, 6 and 24 years for children
 285 and adult; BW: average body weight; 15 and 70 kg for children and adult; AT: the averaging time,
 286 for non-carcinogens, AT (days)=ED×365; for carcinogens, AT (days)=70×365=25, 550.

287 After the D_{inh} was calculated, a Hazard Quotient (HQ) for non-cancer toxic risk can be
 288 obtained by (Kong et al., 2012):

289
$$HQ = D/RfD \quad (4)$$

290 Considering the sensitive group, the reference dose (RfD) (mg/kg/day) is estimated as the
 291 maximum permissible risk on human by daily exposure. The threshold values of RfD indicate
 292 whether there is adverse health effect during a life time. Then Hazard Index (HI) can be obtained
 293 by suming up the individual HQ to estimate the total risks of all elements considered:

294
$$HI = \sum HQ_i \quad (5)$$

295 where i denotes different heavy metals. RfD values are 7×10⁻³, 2.86×10⁻⁵, 1.43×10⁻⁵,
 296 4.0×10⁻², 3.0×10⁻¹ and 3.5×10⁻³ for the cancer risk estimation of V, Cr, Mn, Cu, Zn and Pb. For
 297 non-cancer risk estimation of Co, Ni, As and Cd, the RfD values are 5.71×10⁻⁶, 2.00×10⁻²,
 298 3.00×10⁻⁴ and 1.00×10⁻³, respectively (Kong et al., 2012). If HI≤1, there is no adverse health
 299 effects; if HI>1, likely adverse health effects exist. For carcinogens, the LADD is multiplied by
 300 the corresponding RfD value (they are 9.8×10⁰, 8.4×10⁻¹, 1.51×10¹ and 6.3×10⁰ for Co, Ni, As
 301 and Cd, respectively) (Kong et al., 2012). If the cancer risk is higher than 10⁻⁶, risk management
 302 decisions should be made.

303 2.4.4 Mass closure of PM_{2.5}

304 To better understand the chemical compositions before, during and after SF, the chemical
 305 mass closure analysis was conducted. The chemical components are divided into six classes as
 306 follows: mineral matter (MIN), trace elements (TE), OM, EC, sea salt (SS), secondary inorganic
 307 aerosol (SIA) and unidentified matter (UM). MIN is the sum of the common oxides of Al, Mg, Mn,

308 Si, Na, K, Ca, Ti and Fe as:

$$309 \text{ MIN}=2.14 \times \text{Si}+1.67 \times \text{Ti}+1.89 \times \text{Al}+1.59 \times \text{Mn}+1.67 \times \text{Mg}+1.95 \times \text{Ca}+1.35 \times \text{Na}+1.21 \times \text{K}+1.43 \times \text{Fe} \quad (6)$$

310 As the existence of CaO and CaCO₃, a factor of 1.95 for Ca is used (Terzi et al., 2010).

311 Except for the above elements in MIN, all other elements are summed up to act as TE. OM is
312 calculated by multiplying OC of a conversion factor, in accordance with the organic molecular
313 carbon weight per carbon weight. Here, 2.0 is applied, same to the value used for spring festival
314 period in Shanghai, another megacity in Yangtze River Delta region (Huang et al., 2012). In
315 Allan et al. (2010), during bonfires and fireworks burning period at the Guy Fawkes' night, the
316 OM/OC ratio ranged around 2.0 or higher than 2.0. The marine contribution is calculated based on
317 a standard sea water composition, assuming that soluble Na⁺ in aerosols only come from sea salt.

318 Then,

$$319 \text{ sea salt}=[\text{Na}^+]+[\text{ss-Cl}^-]+[\text{ss-Mg}^{2+}]+[\text{ss-K}^+]+[\text{ss-Ca}^{2+}]+[\text{ss-SO}_4^{2-}] \quad (7)$$

320 where ss-Cl⁻=1.8×[Na⁺], ss-Mg²⁺=0.12×[Na⁺], ss-K⁺=0.036×[Na⁺], ss-Ca²⁺=0.038×[Na⁺], and
321 ss-SO₄²⁻=0.252×[Na⁺] (Terzi et al., 2010). SIA is the sum of nss-SO₄²⁻, NO₃⁻ and NH₄⁺. The
322 concentrations of all these species in μg m⁻³ are adopted.

323 2.4.5 Visibility re-construction by chemical components

324 The mass scattering efficiencies of spherical particles is a function of water and chemical
325 components including (NH₄)₂SO₄, sea salt, mineral materials and carbonaceous species (Kim et al.,
326 2001). To find which types of chemical components are the key for the visibility degradation during
327 sampling period and how can the injection of FW particles change the visibility, the IMPROVE
328 equation was used to calculate the light extinction coefficient (b_{ext}) (Kim et al., 2001; Yang et al.,
329 2007):

$$330 b_{\text{ext}}=3f(\text{RH}) [\text{ammonium sulfate}]+3f(\text{RH}) [\text{ammonium nitrate}]+4[\text{OM}]+1[\text{soil}]+10[\text{BC}] \quad (8)$$

331 The visibility can be calculated by $V_s=3.91/b_{\text{ext}}$ (Yang et al., 2007). We used [ammonium
332 sulfate]=0.944×[NH₄⁺]+1.02×[SO₄²⁻], [ammonium nitrate]=1.29×[NO₃⁻], [OM]=2.0×[OC],
333 [soil]=MIN and [BC]=[EC] (Yang et al., 2007; Tao et al., 2009). f(RH) is the RH growth function
334 indicating how scattering efficiencies increase for SO₄²⁻ and NO₃⁻ as they absorb liquid water and
335 detailed data can be found in Tao et al. (2009).

336 2.4.6 WRF-FLEXPART modeling

337 To see the transport distance and decreasing trend of the highest mass concentrations of

338 PM_{2.5} at CNY's Eve, Weather Research and Forecast model (WRF) version 3.4 was used to
339 provide meteorological inputs of FLEXPART, with the NCEP global reanalysis meteorological
340 dataset (1°×1°) as initial and boundary conditions. The time step is set as 180 s. The grid system is
341 divided into 28 layers in the vertical direction. Two domains are adopted, with the grid resolutions
342 of 30 and 10 km. The simulating time period is 02:00-11:00 of Jan.31, 2014. The output of 10 km
343 evolution wind farms is used as the input of FLEXPART. For forward simulating of FLEXPART
344 model, Nanjing (N31°14'-32°37', E118°22'-119°14', height as 50 m) is considered as a whole
345 source region. In this study, we only considered the dry and wet deposition of particles at CNY's
346 Eve. The average mass concentration of 572 μg m⁻³ is used as the initial particle concentration.

347 **3 Results and discussion**

348 **3.1 Comparison of particles before, during and after Chinese Spring Festival**

349 **3.1.1 PM_{2.5} mass concentrations**

350 The concentrations of PM_{2.5} (averaged as 113±69 μg m⁻³, min-max: 21-318 μg m⁻³) in this
351 study by filter sampling varied consistently with those for the nine online monitoring sites set by
352 local government at urban Nanjing (averaged as 112±70 μg m⁻³, min-max: 13-385 μg m⁻³)
353 (Fig.2b). They correlated well with correlation coefficient (R²) higher than 0.95 (P>0.01)
354 (Supplementary file S6), indicating that a regional air pollution occurred in Nanjing (visibility<10
355 km as Fig.2a shown) during study period. The PM_{2.5} concentrations all peaked at CNY (Jan. 30)
356 and LF (Feb.14) and the peaking values at CNY were 4-5 times of the secondary standard of
357 China National Ambient Air Quality (75 μg m⁻³, 24 h average). Results suggested that FW have
358 obvious impacts on fine particle pollution. At CNY's Eve, two massive FW events usually occur
359 at the evening (around 19:00-20:00 h for the family reunion dinner) and midnight (00:00-02:00 h
360 for celebrating the new year). PM_{2.5} showed the maximum concentrations for the two episodes as
361 426±236 (20:00 h) and 572±136 μg m⁻³ (02:00 h), respectively (Fig.4). After 02:00, obviously
362 decreasing (as exponential form, R²=0.99) was observed. The concentrations decreased to 195±16
363 μg m⁻³ at 13:00, which was similar to that of 178±16 μg m⁻³ at 17:00, Jan. 30 before extensively
364 FW activities (Fig.4). Note that at Jan. 30 and Jan. 31, the mixing layer heights were only 257 and
365 227 m, the wind speeds were 1.7 and 2.1 m s⁻¹ and the RH were 88 and 80%, all favoring the
366 accumulation of pollutants and regional air pollution formation. It was verified by the
367 WRF-FLEXPART results which indicated that the particles with highest mass concentrations at

368 02:00 moved outside of Nanjing in the following nine hours. The center with peaked particle mass
369 concentrations transported about 285 km to the north of Naning ([Supplementary file S7](#)) and the
370 decreasing trend was in accordance with the real particle concentrations decreasing ([Fig.5](#)). The
371 injection of FW particles deteriorated the air quality, with visibilities decreased to 1.4-6.2 km in
372 the following four days. Therefore, the PM_{2.5} pollution raised by FW can last for at about four
373 days under unfavorable weather conditions (visibility was strongly related to PM_{2.5} mass in Jan
374 30-Feb.3, R²=0.82). At Feb.3 and Feb.5, PM_{2.5} was cleaned effectively by the rainfall
375 (precipitation as 0.3 and 9 mm), descreasing by 5.6-10.6 times for the ten sites.

376

377 [\(Fig.4\)](#)

378

379 [\(Fig.5\)](#)

380

381 **3.1.2 Characteristic of chemical species**

382 [Table 1](#) and [Table 2](#) summarized the statistics of PM_{2.5}, water-soluble ions, OC and EC
383 before, during and after SF. The data at CNY and LF were listed separately for intensive FW
384 **activities**. The ratios of PM_{2.5} and chemical species at CNY and LF with those for the day before
385 them were also listed. For elements, K, Si, Al, Na, Ca and Fe were the most abundant species,
386 totally accounting for 85%-90% of all the elements at these five periods. Without considering the
387 data for CNY, elements Al, K, Ba and Sr at SF still elevated when compared with those for Pre-SF,
388 whereas all other elements descreased during SF. This was related to the weakened sources, like
389 construction activities, vehicle emission and industrial activities in the national holiday. For ions,
390 NO₃⁻ was most abundant, averaged as 5.9 (±3.7) µg/m³ for the days without intensive FW
391 activities, then followed by SO₄²⁻ and NH₄⁺, with average concentrations of 5.0 (±3.7) and 4.8
392 (±2.4) µg m⁻³, respectively. K⁺ and Cl⁻ also had relatively high concentrations of 0.9 (±1.0) and 0.8
393 (±0.5) µg m⁻³. It was similar to the results of [Wang et al. \(2014\)](#) that the secondary aerosols in
394 Nanjing were dominated by nitrate in winter haze periods. Na⁺, Ca²⁺, Mg²⁺, F⁻ and NO₂⁻
395 accounted for a minor fraction (totally of 4.2%). For carbonaceous species, OC3, OC4 and EC1
396 were most abundant, in combination accounting for 80% of the total carbon, indicating coal
397 combustion and gasoline exhaust were important sources for PM_{2.5} at Nanjing ([Cao et al., 2005](#)).

398 OPC and OC1 also showed a higher values which may be related to biomass burning (Cao et al.,
399 2005). NO_3^- , OC and EC were highest for Pre-SF period, as the “spring travel rush” effect,
400 characterized by extremely high traffic flows (Huang et al., 2012). The $\text{PM}_{2.5}$ concentrations
401 decreased for about $10 \mu\text{g m}^{-3}$ during SF, implying that the reduction of anthropologic sources in
402 this national holiday (Feng et al., 2012). The particle concentration lower than that for pre-holiday
403 period was also found in Shanghai (Huang et al., 2012).

404 During CNY with intensive FW, concentrations of Ba and Sr exhibited the most significant
405 increase, by factors of 99.1 and 79.4 compared to the day before CNY (Pre-CNY). Ba and Sr also
406 showed the highest ratios for LF/Pre-LF (the day before LF), as 9.7 and 5.7, respectively. Then
407 followed by EC2, OC1, K, K^+ , Al, Bi, SO_4^{2-} , OC2, EC1 and OC, going up to 4.1-37.7 times for
408 CNY/Pre-CNY, respectively. Other species increased by 1.2-3.8 times except for W (0.6), Na^+
409 (0.7), NO_2^- (0.8) and OC4 (0.9). It implied that Na^+ was not affected by the FW and can be used as
410 the tracer of sea salt. Most species also increased at LF when compared with Pre-LF, but the
411 increasing ratios were much lower than those at CNY. It can be explained as the FW activities at
412 LF (there are only organized FW activities by some organizations at cities) were less intensive
413 than those at CNY (FW activities are national spread, from city to small villages). Crustal
414 elements like Li, Be, Si, Na, Ca, Ti and Mn increased by about 1-2 times during FW, indicating
415 the use of clay in firework production. Ca^{2+} and EC1 decreased by factors of 0.8 and 0.9,
416 suggesting the increase of construction activities and vehicle emissions after SF. Meanwhile, Ba
417 and Sr tend to be tracers of firework ($R^2=0.99$), consistent with former studies (Estrellan and Iino,
418 2010; Sarkar et al., 2010; Feng et al., 2012). As shown in the supplementary file S2 and literature
419 (Moreno et al., 2007; Vecchi et al., 2008; Joly et al., 2010; Sarkar et al., 2010; Richard et al., 2011;
420 Do et al., 2012; Tsai et al., 2012; Jing et al., 2014), the compounds of these elements are important
421 FW manufacturing materials. Barium compounds can be used as oxidiser (BaClO_3 and $\text{Ba}(\text{NO}_3)_2$).
422 $\text{Sr}(\text{NO}_3)_2$ can be used to give red color fireworks and potassium compounds are the most
423 important compositions of black powder (as KNO_3 or KClO_3). Al is used alone as a common
424 constituent for fuel, or to form sparks and glitter effects or as alloy magnalium (50:50 Mg:Al) for
425 sparks and crackling stars. Fireworks also contain charcoal (Joly et al., 2010; Sarkar et al., 2010;
426 Tsai et al., 2012) and organic materials are used as adhesive, such as polyvinyl alcohol,
427 polyoxyethylene, phenol formaldehyde resin and shell-lac. They are responsible for the elevated

428 concentrations of EC2 (Joly et al., 2010; Sarkar et al., 2010; Tsai et al., 2012) and OC1 during FW
429 periods.

430

431 (Table 1)

432

433 (Table 2)

434

435 3.2 Mass closure and re-construction of visibility

436 Fig. 6 illustrates the PM_{2.5} mass balance of MIN, TE, OM, EC, SS, SIA and UM. About 60%
437 of the chemical species in PM_{2.5} were detected. The unaccounted PM mass were explained by the
438 following four reasons: (1) non-C atoms in organic aerosols; (2) sampling and measurement
439 artefacts; (3) conversion factors used for OM and MIN calculating; (4) aerosol water content
440 (Tsyro, 2005; Terzi et al., 2010). Water constituted 20-35% of the annual mean PM₁₀ and PM_{2.5}
441 concentrations (Tsyro, 2005). At Feb. 6, the water content in PM_{2.5} was high to 72%, indicating
442 the influence of rainfall and high RH (90%). These also lead to the gravimetrically measured
443 particulate mass (PM_{meas}) higher than the mass calculated by adding individual components
444 (PM_{meas}), while tight correlations still existed between them ($PM_{meas}=1.52PM_{cal}+14.5$, $R^2=0.91$).
445 The slope was similar to those as 1.02-1.42 in Terzi et al. (2010).

446

447 (Fig.6)

448

449 The averaged chemical components of PM_{2.5} profiles exhibited OM (26%)>SIA (18%)>MIN
450 (9%)>EC (3.9%)>SS (1.7%)>TE (0.67%). The mass percentages of OM, TE and EC decreased in
451 SF (as 23%, 0.6% and 2.7%) when compared with those at Pre-SF (as 34%, 0.7% and 6.2%).
452 These changes reflected the holiday effect i.e. at the SF holiday, the new injection of FW particles
453 cannot offset the reduced particles from vehicle emission and/or to industrial sources, especially
454 for organic matter, trace elements and elemental carbon, which are important compositions of
455 vehicle exhausts and industrial activities. At CNY, obviously elevated OM was observed,
456 accounting for 39.3% of PM_{2.5}. While SIA was only 14.4%, with the peak values occurred at
457 Feb.3 (as 36%), suggesting that after intensive emission of FW pollutants at CNY's Eve,

458 secondary ions were gradually formed during aging processes through gas-particles transformation
459 of SO₂ and NO_x, etc. It should be emphasized that MIN and TE were both important compositions
460 of PM_{2.5}, totally accounting for 5.8%-18.5%. In a recent study by AMS for aerosols during
461 Chinese Spring Festival at Beijing, organics, nitrate, sulfate, ammonium, BC and chloride,
462 accounted for 43%, 22%, 14%, 13%, 5% and 3% of PM_{1.0} with no elements considered (Jiang et
463 al., 2014). The combination of filter sampling-offline chemical analysis and online real-time
464 monitoring of chemical species are desired for atmospheric aerosol studies.

465 Fig. 7a shows the calculated average values of extinction coefficient (b_{ext}). They varied
466 between 44 and 525 Mm⁻¹. The calculated visibility (V_{cal}) exhibited good correlations with the
467 measured one (V_{meas}) ($V_{cal}=0.96V_{meas}+1.4$, $R^2=0.45$, $P<0.001$). The discrepancy between the
468 measured and calculated values can be attributed to the influence of ambient water vapor (Huang
469 et al., 2012) which was a key component of aerosol particles in this study as discussed before. At
470 higher RH, the role of ambient water vapor on light extinction was more important (Huang et al.,
471 2012). The b_{ext} exhibited higher values at CNY and the following three days, in the range of
472 301-525 Mm⁻¹. (NH₄)₂SO₄ had the largest contribution to b_{ext} , accounting for 36.5±1.7%,
473 followed by NH₄NO₃ (25.8±8.2%), EC (21.8±9.0%), OM (10.8±4.2%) and soil (5.1±1.8%)
474 (Fig.7b). These results implied that sulfate was the largest contributor to visibility degradation
475 especially at SF period. Before SF, the contribution of EC can be as high as 34%-44% during
476 serious haze periods (Jan. 24-26, RH<51%). It highlights the importance of controlling vehicle
477 emissions in haze days. Sulfate and soot were also found as the main contributors to visibility
478 degradation in other studies (Tao et al., 2009). The results obtained here were different from those
479 in Shanghai that organic aerosol had the largest contribution to the aerosol extinction as 47 %,
480 then followed by ammonium sulfate (22%), ammonium nitrate (14 %) and EC (12 %) (Huang et
481 al., 2012). The FW at CNY obviously changed the contributions of chemical species to scattering
482 coefficient. At CNY, the influence of FW particles on visibility was mainly controlled by
483 (NH₄)₂SO₄ (36%), NH₄NO₃ (26%), EC (15%) and OM (15%). During FW particle aging
484 processes, the contribution of (NH₄)₂SO₄ increased from 36% (Jan.30) to 67% (Feb.3), while for
485 NH₄NO₃, its contribution increased first to 28% at Jan.31 and then decreased to 10% (Feb.3).
486 Similar trend was found for EC, it increased to 22% (Feb.1) and then decreased to 7.6% (Feb.3).
487 For OM, it exhibited decreasing trend, to the lowest value at Feb.2 (5.5%).

488

489 (Fig.7)

490

491 3.3 Source evolution

492 3.3.1 Contributions of fireworks burning to PM_{2.5} at CNY and LF

493 The PM_{2.5} concentrations peaked at CNY and LF in this study with intensive FW activities.
494 Assuming that the PM_{2.5} collected on CNY and LF was a simple combination of particles from
495 FW and other emission sources, the contribution and compositions of the particles from FW can
496 be estimated by subtracting the contribution of the non-firework sources (Feng et al., 2012). An
497 accumulation factor of 0.88 (mixing layer heights at Jan. 30 and Jan. 29 were 227 and 257 m,
498 respectively) and 0.51 (mixing layer heights at Feb. 14 and Feb. 13 were 353 and 696 m,
499 respectively) were used to eliminate the disperse impact caused by mixing height layer increasing
500 (Feng et al., 2012; Deka and Hoque, 2014). About 60.1% and 10.9% of the PM_{2.5} masses at CNY
501 and LF were estimated to be from FW. The contributions to almost all species of FW at CNY were
502 more obvious than those at LF (Fig.8). At CNY, OPC, EC3, Ba, Sr, Soot-EC, EC2 and OC1
503 maintained the higher contributions from FW, larger than 80%, followed by K, K⁺, Al, Bi and
504 Char-EC, with the contributions higher than 70%. At LF, 45% of Ba and 41% of Sr were from FW
505 and the contributions to V, Bi, Fe, Be, K, K⁺, Al, NO₂⁻ and Sb were higher than 20%.

506

507 (Fig.8)

508

509 3.3.2 Source variations by tracers and PCA analysis

510 In order to further identify the sources of particles, PCA results are shown in Fig.9 and
511 supplementary file S8.

512

513 (Fig.9)

514

515 Five, five and eight factors were extracted for the dataset of Pre-SF, SF and After-SF period,
516 which explained 100%, 99.4% and 97.5% of the variance, suggesting almost all the sources have
517 been explained. Fireworks burning was the most important source for PM_{2.5}, contributing 24.0%

518 for the whole period. Coal combustion (including both local and regional transport) was also
519 important to PM_{2.5} at this site in winter (contributing 19.3%). It was verified by the time series of
520 tracers (As and Sb, highly correlated with R²=0.88) for coal combustion in Fig.10a. Extremely high
521 values can be found at Jan. 24, even higher than those for the intensive FW day. This can be
522 explained by two reasons: (1) on Jan. 24, it was a haze day with visibility and mixing layer height
523 as 8.2 km and 321 m, facilitating the accumulation of pollutants; (2) the air masses on Jan.24 were
524 classified as cluster 2 from central China where the Chang-Zhu-Tan region with intensive
525 non-ferrous metal metallurgy industries with huge coal consumption is located. On this day,
526 higher concentrations were also found for metals like Mg (228 ng m⁻³), Cr (17 ng m⁻³), Ca (782 ng
527 m⁻³), Mn (85 ng m⁻³), Fe (1014 ng m⁻³), Co (0.61 ng m⁻³), Ni (7.6 ng m⁻³), Cu (124 ng m⁻³), Mo
528 (4.4 ng m⁻³), Cd (8.8 ng m⁻³), Sn (16 ng m⁻³) and Pb (359 ng m⁻³). FW contributed about half of
529 the PM_{2.5} during SF period. For Pre-SF and after-SF periods, its contributions were 9% and 14%.
530 As shown in Fig.10b, the tracers of Ba and Sr exhibited much higher values at SF, and there were
531 also some small peaks before SF (Jan. 27) and after SF (Feb. 14). During the one-week holiday,
532 most industrial activities shut down in China with low energy consumption during this period
533 (Feng et al., 2012; Huang et al., 2012; Li et al., 2013). As holiday effect, when compared the
534 source contributions at SF to those at Pre-SF, the contributions of coal combustion decreased from
535 46% to only 16%, the contributions of vehicle emissions decreased from 17% to 14% and the
536 contributions of dust also decreased. For After-SF period, along with the gradually re-starting of
537 industrial plants and construction activities and increasing traffic density, the contributions for coal
538 combustion, heavy oil burning, industrial processes and road dust increased, to 37%, 4%, 3.4%
539 and 5%, respectively. OC and EC were selected as the tracers of vehicle emission and their
540 correlation was higher to 0.80 without the data at CNY and LF. Ca was selected as the tracer for
541 construction activities or road dust (the main road was covered by abundant dust from subway
542 construction). Na⁺ was used as the tracer of sea salt. Li, Be and Si were selected as the indicators
543 of soil (R² higher than 0.65 between them). The variations of mass concentrations of these tracers
544 before, during and after SF coincided with the contributions of corresponding sources.

545

546

(Fig.10)

547

548 3.4 Aging processes

549 3.4.1 The aging processes and mechanisms of fireworks burning particles

550 Previous studies indicated that the aerosol emission from FW activities is a short-term air
551 quality degradation event (Jing et al., 2014), but no studies concerned how long the duration time
552 is, and during the aging processes, what are the substantial hazard risk levels raised by elevated
553 heavy metals from intensive FW. To better understand the influence of FW particles, its aging
554 processes after emission were analyzed. It should be emphasized that at SF, contributions from
555 other human sources were low (Fig.9), so the air quality in these days was mainly influenced by
556 the highest contributor-FW particles' aging processes, including deposition, dispersion and
557 transformations.

558 From Fig.2b and Fig.10b, it can be seen that it takes about four days for the highest PM_{2.5} and
559 FW tracers-Ba and Sr at CNY to step down to the normal values of pre-CNY. The same situations
560 were found for K⁺, Cl⁻, NH₄⁺ and NO₃⁻ (Fig.11a). For SO₄²⁻, at Feb.3, its mass concentrations
561 decreased to a lower level of 6.1 μg m⁻³. Then at Feb.4, it did not decrease immediately to the
562 level of Jan. 29 until a rainfall (9 mm) at Feb.5. New emissions related with scattered fireworks
563 burning at surroundings were thought to be introduced at Feb.4 as Ba, Sr, K⁺, Ca²⁺, Ca and Na⁺
564 (they are all from primary emissions) slightly increased at Feb.4. Therefore, the variations of SO₄²⁻
565 at Feb.5 may not just related with the aging of the intensive FW particles at CNY's Eve. On Feb.1,
566 though PM_{2.5} has decreased from 317 to 185 μg m⁻³, the visibility was still low as 2.2 km, with
567 peak concentrations of NH₄⁺, NO₃⁻ and SO₄²⁻ (they contributed 65% to the b_{ext}). On Feb.3, PM_{2.5}
568 decreased to 30 μg m⁻³, haze pollution still existed with the visibility as 6.7 km, mainly
569 contributed by ammonium sulfate (67%). It can be preliminarily concluded that the intensive FW
570 particles at CNY's Eve can influence the air quality for at about four days by changing the main
571 contributors of extinction coefficient from EC+OM to ammonium sulfate. Drewnick et al. (2006)
572 also found that after about three or four days, though the aerosol mass concentrations dropped to
573 about one-third of the concentrations for Near Year's firework burning period, the relative
574 compositions of aerosols were similar. And the mass concentrations of nitrate, sulfate and
575 ammonium increased again after about three days.

576

577 (Fig.11)

578

579 Pollution gases (SO_2 , NO_x , etc.) emitted during FW events may be oxidized to secondary
580 organic and inorganic components that may be adsorbed onto particles (Sarkar et al., 2010). From
581 Fig.11a, we can find that Ca^{2+} , NH_4^+ , NO_3^- and SO_4^{2-} showed peak values at CNY and two days
582 after, suggesting the directly emission from FW and secondary formations through heterogeneous
583 reactions of SO_2 and NO_x on crustal materials. Higher correlations were found for NO_3^- - Ca^{2+}
584 ($R^2=0.64$) and SO_4^{2-} - Ca^{2+} ($R^2=0.70$). The lower wind speed ($1.7\text{-}2.6\text{ m s}^{-1}$) and mixing layer
585 heights (257-284 m) helped to capture pollution gases near the ground and higher RH (74%-88%)
586 favored their secondary transformation and following condensation onto pre-existing aerosols at
587 the initial four days after intensive FW emissions on CNY.

588 From Jan. 30 to Feb. 4, the ratios of soot-EC/ NO_3^- , Cl^-/K^+ , $\text{NO}_3^-/\text{SO}_4^{2-}$ and Ca^{2+} decreased
589 first and then increased again, while to the opposite for $\text{SO}_4^{2-}/\text{K}^+$, suggesting the secondary
590 formation (Fig.11b). Secondary formations of NH_4^+ , NO_3^- and SO_4^{2-} from the gases emitted from
591 FW were also found in other cities (Wang et al., 2007; Yang et al., 2014). During aging, the direct
592 emission of KCl from fireworks (Drewnick et al., 2006) ($R^2=0.85$ for K^+ -Cl) can react with
593 H_2SO_4 and HNO_3 to form SO_4^{2-} ($R^2=0.76$ for K^+ - SO_4^{2-}) and NO_3^- ($R^2=0.96$ for K^+ - NO_3^-), leading
594 to the decreasing of Cl^-/K^+ ratio and increasing of $\text{SO}_4^{2-}/\text{K}^+$ ratio. Li et al. (2013) drew the same
595 conclusion through single particle analysis as that K-rich particles containing significant amounts
596 of S in the form of K_2SO_4 at a background site under the influence of FW. It implied the existence
597 of the aging of fresh FW particles via heterogeneous reactions during long-range transport. Soot
598 (soot-EC) can be directly introduced by firework displays (Do et al., 2012) which showed
599 moderate correlations with NO_3^- and SO_4^{2-} ($R^2=0.47$ and 0.56 , respectively) in this study,
600 indicating the coating of NO_3^- and SO_4^{2-} on soot. The OC/EC ratio peaked on CNY (as 6.8) which
601 was mainly contributed by the increasing of OC1, OC2 and OPC. They are related with
602 volatilization of the organic materials used for fireworks producing. The smelting point
603 temperatures for polyvinyl alcohol, polyoxyethylene and shell-lac are $230\text{-}240^\circ\text{C}$, 212°C ,
604 $115\text{-}120^\circ\text{C}$ and the softening point for phenol formaldehyde resin is $80\text{-}85^\circ\text{C}$, all lower than the
605 detecting temperature for OC2 (230°C). Therefore, OC1, OC2 and OPC are more easily and
606 directly emitted from FW. The initially decreasing OC/EC ratio indicated the gradual formation
607 of secondary (aged) organic aerosols (Feng et al., 2012). To summarize, the heterogeneous

608 reactions of SO_2 and NO_x on crustal materials directly from FW, the replacement of Cl^- by NO_3^-
609 and SO_4^{2-} , coating of NO_3^- and SO_4^{2-} on soot and formation of secondary organic aerosols are the
610 main aging mechanisms of FW particles.

611 Previous studies also **indicated** that metals like Fe, Cu and Mn can catalyze the formation of
612 NO_3^- and SO_4^{2-} (Wang et al., 2007; Do et al., 2012; Feng et al., 2012). Wang et al. (2007)
613 indicated that the heterogeneous formation of sulfate through reacting with $\alpha\text{-Fe}_2\text{O}_3$ existed under
614 moist atmosphere and was a function of RH and HNO_3 . As shown in Fig.12 and Supplementary
615 file S9, **significant** correlations are found between NO_3^- and Fe, Cu and Mn and between SO_4^{2-} and
616 Fe, Cu and Mn at higher RH. It indicated the mechanism of metal-catalyzed formation of NO_3^-
617 and SO_4^{2-} was more likely to occur at higher RH. At the day of CNY and Feb.2, the RH was 88%
618 and 87%, implying the occurrence of metal-catalyzed reactions, which may also explain the higher
619 NO_3^- and SO_4^{2-} concentrations at these days. The R^2 increased with the elevated RH. There are
620 **obvious** increases of R^2 for Fe- NO_3^- , Mn- NO_3^- and Cu- NO_3^- when RH were >85%, >85%
621 and >65%, respectively. For the correlations of Fe- SO_4^{2-} , Mn- SO_4^{2-} and Cu- SO_4^{2-} , clear
622 increasings in R^2 were found when RH were >85%, >85% and >55%. Then we can conclude that
623 for Fe-catalyzed and Mn-catalyzed reactions, the threshold of RH was around 85%; for
624 Cu-catalyzed formation of NO_3^- and SO_4^{2-} , the thresholds of RH were around 65% and 55%,
625 respectively. For RH higher than 90%, R^2 decreased for Fe- NO_3^- , Cu- NO_3^- , Fe- SO_4^{2-} and
626 Mn- SO_4^{2-} which needs more data in the future to be verified and explained.

627

628 (Fig.12)

629

630 3.4.2 Potential health risks during the aging of fireworks burning particles

631 After emitted from the intensive FW at CNY's Eve, heavy metals including Vi, Cr, Mn, Co,
632 Ni, Cu, Zn, As, Cd and Pb decreased directly in the following four days (Supplementary file S10).
633 It indicated that they were emitted from FW primarily and were removed mainly by dispersion and
634 deposition during aging. Then we can assume that: (1) other emission sources (coal combustion,
635 vehicle exhaust and industrial processes were their main sources) for these metals were stable
636 during SF period; (2) the highest concentrations of them were just the combinations of particles
637 from the FW on Jan. 30 and other sources on Jan. 29. We subtract the concentrations of elements

638 at Jan. 29 from the corresponding values on Jan.30, Jan.31, Feb.1 and Feb.2 for each element,
639 respectively, to obtain the element concentrations just related with the FW particles. Considering
640 the variations of mixing layer height (as 306, 257, 227, 284 and 248 m for the five days of
641 Jan.29-Feb.2) and accumulation effect, the concentrations of these elements on Jan. 30, Jan.31,
642 Feb.1 and Feb.2 were transferred by factors of 0.84, 0.74, 0.93 and 0.81, respectively. Then the
643 $C_{95\%UCL}$ values raised by FW particles were 7.4, 21.2, 12.0, 23.7, 0.42, 5.2, 54.5, 11.7, 126 and
644 837 ng m^{-3} of the ten elements, respectively, for the four days. The non-cancer risks raised just by
645 FW particles at CNY's Eve were below 1 (0.03 and 0.02 for children and adult) (Fig.13),
646 indicating no adverse health effects. However the cancer risk was 1.62×10^{-6} , higher than 10^{-6} ,
647 suggesting the FW particles were important carcinogens and should be controlled effectively
648 especially for the contained Cd and As. Meanwhile, the risk level for children was higher than that
649 for adult, which meant that children were more sensitive to non-carcinogenic effects and should be
650 kept from possible exposure to them (Yang et al., 2014). The FW should be restricted at SF from
651 the view of their cancer risks to human health.

652

653 (Fig.13)

654

655 **4 Conclusions**

656 Thirty-nine elements, ten water-soluble ions and eight fractions of carbonaceous species were
657 measured to fully characterize the chemical compositions in atmospheric $PM_{2.5}$ in Nanjing during
658 the 2014 Chinese Spring Festival (SF). Serious regional haze pollution occurred and lasted during
659 the whole sampling period. At the Chinese New Year (CNY)'s Eve, after it peaked at 02:00, $PM_{2.5}$
660 exponentially decreased in the following 11 hours to the level before extensive fireworks burning
661 (FW) activities. Due to holiday effect, almost all elements decreased during SF except for Al, K, Ba
662 and Sr which were related with FW. As the "spring travel rush" effect, NO_3^- , OC and EC showed
663 highest values for periods before SF, indicating the extremely high traffic flows. At the New
664 Year's Eve, about 60.1% of the $PM_{2.5}$ mass was estimated to be from FW. Highly elevated Ba and
665 Sr were also found (highly correlated with each other), indicating they can be used as the tracers
666 of FW. The intensive FW at CNY's Eve obviously changed the chemical compositions of $PM_{2.5}$,
667 with elevated organic matter (OM) immediately, contributing 39.3% of $PM_{2.5}$. The contributions

668 of secondary ions formed by gas-particle transformations gradually increased during FW particles'
669 aging processes. After FW particles emitted at CNY, the contribution of $(\text{NH}_4)_2\text{SO}_4$ to extinction
670 coefficient increased from 36% to 67%; while for NH_4NO_3 and EC, their contributions increased
671 first and then decreased. According to tracers and principle component analysis, fireworks burning
672 was the most important source of $\text{PM}_{2.5}$ at this site. They contributed about half of $\text{PM}_{2.5}$ during
673 SF. Tracers for various sources (As and Sb for coal combustion, Ba and Sr for FW, OC and EC for
674 vehicle emission, Ca for construction or road dust, Na^+ for sea salt and Li, Be and Si for soil)
675 performed well and they varied accordantly with the contributions of corresponding sources. The
676 FW particles emitted from CNY's Eve may undergo about four days' aging processes from the
677 variations of Ba, Sr, NH_4^+ , NO_3^- , SO_4^{2-} and K^+ . The aging processes were characterized by
678 heterogeneous reactions of SO_2 and NO_x on crustal materials directly from FW, the replacement of
679 Cl^- by NO_3^- and SO_4^{2-} , coating of NO_3^- and SO_4^{2-} on soot, formation of secondary organic aerosols
680 and metal-catalyzed formation of NO_3^- and SO_4^{2-} at higher relative humidity. For Fe-catalyzed and
681 Mn-catalyzed reactions, the thresholds of RH were around 85%; while for Cu-catalyzed formations
682 of NO_3^- and SO_4^{2-} , the thresholds of RH were around 65% and 55%, respectively. During the
683 aging processes, FW particles at CNY obviously changed the main contributors to the extinction
684 coefficient from EC+OM to ammonium sulfate. Meanwhile, higher cancer risks raised by heavy
685 metals (especially for Cd and As) only related with FW particles emitted at CNY's Eve was
686 1.62×10^{-6} , which also imposed higher non-cancer risks to children than adult. The results in this
687 study will be useful for understanding the detailed compositions and aging processes of FW
688 particles and also highlight the importance of controlling intensive fireworks burning in order to
689 protect air quality and reduce the cancer risks.

690

691 **Acknowledgment.** This work was funded by the National Natural Sciences Foundation of China
692 (No. 41030962), Scientific and technological cooperation between the Government of
693 China-Serbia (2013(158)2-10), the grant of China Scholarship Council and the Priority Academic
694 Program Development (PAPD) of Jiangsu Higher Education Institution.

695

696 **References**

697 Allan, J. D., Williams, P. I., Morgan, W. T., Martin, C. L., Flynn, M. J., Lee, J., Nemitz, E.,
698 Phillips, G. J., Gallagher, M.W., and Coe, H.: Contributions from transport, solid fuel

699 burning and cooking to primary organic aerosols in two UK cities, *Atmos. Chem. Phys.*, 10,
700 647-668, doi:10.5194/acp-10-647-2010, 2010.

701 Attri, A. K., Kumar, U., and Jain, V. K.: Microclimate: formation of ozone by fireworks, *Nature*,
702 411, 1015, 2001.

703 Cao, J. J., Wu, F., Chow, J. C., Lee, S. C., Li, Y., Chen, S.W., An, Z. S., Fung, K. K., Watson, J.
704 G., Zhu, C. S., and Liu, S. X.: Characterization and source apportionment of atmospheric
705 organic and elemental carbon during fall and winter of 2003 in Xi'an, China, *Atmos. Chem.*
706 *Phys.*, 5, 3127-3137, doi:10.5194/acp-5-3127-2005, 2005.

707 Deka, P., and Hoque, R.R.: Incremental effect of festive biomass burning on wintertime PM₁₀ in
708 Brahmaputra Valley of Northeast India, *Atmos. Res.*, 143, 380-391, 2014.

709 Do, T. M., Wang, C.F., Hsieh, Y. K., and Hsieh, H. F.: Metals Present in Ambient Air before and
710 after a Firework Festival in Yanshui, Tainan, Taiwan, *Aerosol Air Qual. Res.*, 12, 981-993,
711 2012.

712 **Drewnck, F., Hings, S. S., Curtius, J., Eerdekens, G., and Williams, J.: Measurement of**
713 **fine particulate and gas-phase species during the New Year's Fireworks 2005 in Mainz,**
714 **Germany, *Atmos. Environ.*, 40, 4316-4326, 2006.**

715 Dutschke, A., Lohrer, C., Kurth, L., Seeger, S., Barthel, M., and Panne, U.: Aerosol Emissions
716 from Outdoor Firework Displays. *Chem. Eng. Technol.*, 12, 2044-2050, 2011.

717 Estrellan, C. R., and Iino, F.: Toxic emissions from open burning, *Chemosphere*, 80, 193-207,
718 2010.

719 Feng, J. L., Sun, P., Hu, X. L., Zhao, W., Wu, M. H., and Fu, J. M.: The chemical composition and
720 sources of PM_{2.5} during the 2009 Chinese New Year's holiday in Shanghai, *Atmos. Res.*, 118,
721 435-444, 2012.

722 Godri, K. J., Green, D. C., Fuller, G. W., OSTO, M. D., Beddows, D. C., Kelly, F. J., Harrison, R.
723 M., and Mudway, I. S.: Particulate Oxidative Burden Associated with Firework Activity,
724 *Environ. Sci. Technol.*, 44, 8295-8301, 2010.

725 Han, Y. M., Cao, J. J., Lee, S. C., Ho, K. F., and An, Z. S.: Different characteristics of char and
726 soot in the atmosphere and their ratio as an indicator for source identification in Xi'an, China,
727 *Atmos. Chem. Phys.*, 10, 595-607, doi:10.5194/acp-10-595-2010, 2010.

728 Han, Y. M., Han, Z. W., Cao, J. J., Chow, J. C., Watson, J. G., An, Z. S., Liu, S. X., and Zhang, R.
729 J.: Distribution and origin of carbonaceous aerosol over a rural high-mountain lake area,
730 Northern China and its transport significance, *Atmos. Environ.*, 42, 2405-2414, 2008.

731 Huang, K., Zhuang, G.S., Lin, Y., Wang, Q., Fu, J. S., Zhang, R., Li, Deng, J. C., and Fu, Q.Y.:
732 Impact of anthropogenic emission on air quality over a megacity-revealed from an intensive
733 atmospheric campaign during the Chinese Spring Festival, *Atmos. Chem. Phys.*, 12,
734 11631-11645, doi:10.5194/acp-12-11631-2012, 2012.

735 Jiang, Q., Sun, Y. L., Wang, Z., and Yin, Y.: Aerosol composition and sources during the Chinese
736 Spring Festival: fireworks, secondary aerosol, and holiday effects, *Atmos. Chem. Phys.*
737 *Discuss.*, 14, 20617-20646, doi:10.5194/acpd-14-20617-2014, 2014.

738 Jing, H., Li, Y. F., Zhao, J.T., Li, B., Sun, J. L., Chen, R. Gao, Y. X., and Chen, C. Y.: Wide-range
739 particle characterization and elemental concentration in Beijing aerosol during the 2013
740 Spring Festival, *Environ. Pollut.*, 192, 204-211, 2014.

741 Joly, A., Smargiassi, A., Kosatsky, T., Fournier, M., Dabek-Zlotorzynska, E., Celio, V., Mathieu,
742 D., Servranckx, R., D'amours, R., Malo, A., and Brook, J.: Characterisation of particulate

743 exposure during fireworks displays, *Atmos. Environ.*, 44, 4325-4329, 2010.

744 Kang, H. Q., Zhu, B., Su, J. F., Wang, H. L., Zhang, Q. C., and Wang, F.: Analysis of a
745 long-lasting haze episode in Nanjing, China, *Atmos. Res.*, 120-121, 78-87, 2013.

746 Kim, K. W., Kim, Y. J., Oh, S. J.: Visibility impairment during Yellow Sand periods in the urban
747 atmosphere of Kwangju, Korea, *Atmos. Environ.*, 35, 5157-5167, 2001.

748 Kong, S. F., Ji, Y. Q., Lu, B., Zhao, X. Y., Chen, L., Bai, Z. P., Xu, Y. H., Liu, Y., and Jiang, H.:
749 Characteristic of PM_{2.5}, PM₁₀ and TSP source profiles for fugitive dust in a coastal oilfield
750 city, China, *Aerosol Air Qual. Res.*, 14, 2017-2028, 2014a.

751 Kong, S. F., Wen, B., Chen, K., Yin, Y., Li, Q., Li, L., Yuan, L., and Sun, X.: Ion chemistry for
752 atmospheric size-segregated aerosol and depositions at an offshore site of Yangtze River
753 Delta (YRD) region, China, *Atmos. Res.*, 147-148, 205-226, 2014b.

754 Kong, S. F., Han, B., Bai, Z. P., Chen, L., Shi, J. W., and Xu, Z.: Receptor modeling of PM_{2.5},
755 PM₁₀ and TSP in different seasons and long-range transport analysis at a coastal site of
756 Tianjin, China, *Sci. Total Environ.*, 408, 4681-4694, 2010.

757 Kong, S. F., Lu, B., Ji, Y. Q., Zhao, X. Y., Bai, Z. P., Xu, Y. H., Liu, Y., and Jiang, H.: Risk
758 assessment of heavy metals in road and soil dust within PM_{2.5}, PM₁₀ and PM₁₀₀ fractions in
759 Dongying city, Shandong Province, China, *J. Environ. Monito.*, 14, 791-803, 2012.

760 Li, L., Yin, Y., Kong, S. F., Wen, B., Chen, K., Yuan, L., and Li, Q.: Altitudinal effect to the size
761 distribution of water soluble inorganic ions in PM at Huangshan, China, *Atmos. Environ.*, 98,
762 242-252, 2014.

763 Li, M. N., and Zhang, L.: Haze in China: Current and future challenges, *Environ. Pollut.*, 189,
764 85-86, 2014.

765 Li, P. H., Han, B., Huo, J., Lu, B., Ding, X., Chen, L., Kong, S. F., Bai, Z. P., and Wang, B.:
766 Characterization, meteorological influences and source identification of carbonaceous aerosol
767 during autumn-winter period in Tianjin, China, *Aerosol Air Qual. Res.*, 2, 283-294, 2012.

768 Li, W. J., Shi, Z. B., Yan, C., Yang, L. X., Dong, C., and Wang, W. X.: Individual metal-bearing
769 particles in a regional haze caused by firecracker and firework emissions, *Sci. Total Environ.*,
770 443, 464-469, 2013.

771 Moreno, T., Querol, X., Alastuey, A., Minguillón, M. C., Pey, J., Rodriguez, S., Miró, J. V., Felis,
772 C., and Gibbons, W.: Recreational atmospheric pollution episodes: Inhalable metalliferous
773 particles from firework displays, *Atmos. Environ.*, 41, 913-922, 2007.

774 Richard, A., Gianini, M. F. D., Mohr, C., Furger, M., Bukowiecki, N., Minguillón, M. C.,
775 Lienemann, P., Flechsig, U., Appel, K., DeCarlo, P. F., Heringa, M. F., Chirico, R.,
776 Baltensperger, U., and Prévôt, A. S. H.: Source apportionment of size and time resolved trace
777 elements and organic aerosols from an urban courtyard site in Switzerland, *Atmos. Chem.*
778 *Phys.*, 11, 8945-8963, doi:10.5194/acp-11-8945-2011, 2011.

779 Sarkar, S., Khillare, P. S., Jyethi, D. S., Hasan, A., and Parween, M.: Chemical speciation of
780 respirable suspended particulate matter during a major firework festival in India, *J. Hazard.*
781 *Mater.*, 184, 321-330, 2010.

782 Shen, Z. X., Cao, J. J., Arimoto, R., Han, Z. W., Zhang, R. J., Han, Y. M., Liu, S. X., Okuda, T.,
783 Nakao, S., and Tanaka, S.: Ionic composition of TSP and PM_{2.5} during dust storms and air
784 pollution episodes at Xi'an, China, *Atmos. Environ.*, 43, 2911-2918, 2009.

785 Tan, P. H., Chou, C., Liang, J. Y., Chou, C. C. K., and Shiu, C. J.: Air pollution "holiday effect"
786 resulting from the Chinese New Year, *Atmos. Environ.*, 43, 2114-2124, 2009.

787 Tao, J., Ho, K. F., Chen, L. G., Zhu, L. H., Han, J. L., Xu, Z. C.: Effect of chemical composition of
788 PM_{2.5} on visibility in Guangzhou, China, 2007 spring. *Particuology*, 7, 68-75, 2009.

789 Terzi, E., Argyropoulos, G., Bougatioti, A., Mihalopoulos, N., Nikolaou, K., and Samara, C.:
790 Chemical composition and mass closure of ambient PM₁₀ at urban sites, *Atmos. Environ.*, 44,
791 2231-2239, 2010.

792 Tian, Y. Z., Wang, J., Peng, X., Shi, G. L., and Feng, Y. C.: Estimation of direct and indirect
793 impacts of fireworks on the physicochemical characteristics of atmospheric fine and coarse
794 particles, *Atmos. Chem. Phys.*, 14, 9469-9479, doi:10.5194/acp-14-9469-2014, 2014.

795 Tsai, H. H., Chien, L. H., Yuan, C. S., Lin, Y. C., Jen, Y. H., and Ie, I. R.: Influences of fireworks
796 on chemical characteristics of atmospheric fine and coarse particles during Taiwan's Lantern
797 Festival, *Atmos. Environ.*, 62, 256-264, 2012.

798 Tsyro, S. G.: To what extent can aerosol water explain the discrepancy between model calculated
799 and gravimetric PM₁₀ and PM_{2.5}, *Atmos. Chem. Phys.*, 5, 515-532, 2005.

800 Vecchi, R., Bernardoni, V., Cricchio, D., Alessandro, A. D., Fermo, P., Lucarelli, F., Nava, S.,
801 Piazzalunga, A., and Valli, G.: The impact of fireworks on airborne particles. *Atmos.*
802 *Environ.*, 42, 1121-1132, 2008.

803 Wang, H. L., An, J. L., Shen, L. J., Zhu, B., Pan, C., Liu, Z. R., Liu, X. H., Duan, Q., Liu, X.,
804 Wang, Y. S.: Mechanism for the formation and microphysical characteristics of submicron
805 aerosol during heavy haze pollution episode in the Yangtze River Delta, China, *Sci. Total*
806 *Environ.*, 490, 501-508, 2014.

807 Wang, Q. Y., Cao, J. J., Shen, Z. X., Tao, J., Xiao, S., Luo, L., He, Q. Y., and Tang, X. Y.:
808 Chemical characteristics of PM_{2.5} during dust storms and air pollution events in Chengdu,
809 China, *Particuology* 11, 70-77, 2013.

810 Wang, Y., Zhuang, G. S., Xu, C., and An, Z. S.: The air pollution caused by the burning of
811 fireworks during the lantern festival in Beijing, *Atmos. Environ.*, 41, 417-431, 2007.

812 Wehner, B., Wiedensohler, A., and Heintzenberg, J.: Submicrometer aerosol size distribution and
813 mass concentration of the millennium fireworks 2000 in Leipzig, Germany, *J. Aerosol Sci.*,
814 12, 1489-1493, 2000.

815 **Williams, J., Drewnick, F., Hings, S.S., Curtius, J., Eerdekens, G., Klüpfel, T., and Wagner, T.:**
816 **Firework emissions for Satellite Validation? *Environ. Chem.*, 2, 94-95, 2005.**

817 Yang, L. X., Gao, X. M., Wang, X. F., Nie, W., Wang, J., Gao, R., Xu, P. J., Shou, Y. P., Zhang,
818 Q. Z., and Wang, W. X.: Impacts of firecracker burning on aerosol chemical characteristics
819 and human health risk levels during the Chinese New Year Celebration in Jinan, China, *Sci.*
820 *Total Environ.*, 476-477, 57-64, 2014.

821 Yang, L. X., Wang, D. C., Cheng, S. H., Wang, Z., Zhou, Y., Zhou, X. H., and Wang, W. X.:
822 Influence of meteorological conditions and particulate matter on visual range impairment in
823 Jinan, China, *Sci. Total Environ.*, 383, 164-173, 2007.

824 Ye, C., Chen, R. S., and Young, C.: Nian: when Chinese mythology affects air pollution, *The*
825 *Lancet*, 9935, 2125, 2014.

826 Yu, X. N., Shi, C. Z., Ma, J., Zhu, B., Li, M., Wang, J., Yang, S. Y., and Kang, N.: Aerosol optical
827 properties during firework, biomass burning and dust episodes in Beijing, *Atmos. Environ.*,
828 81, 475-484, 2013.

829 Zhang, M., Wang, X. M., Chen, J. M., Cheng, T. T., Wang, T., Yang, X., Gong, Y. G., Geng, F.
830 H., and Chen, C. H.: Physical characterization of aerosol particles during the Chinese New

831 Year's firework events, Atmos. Environ., 44, 5191-5198, 2010.

832

833

834

835

836

837

838

839

840

841

842

843

844

845

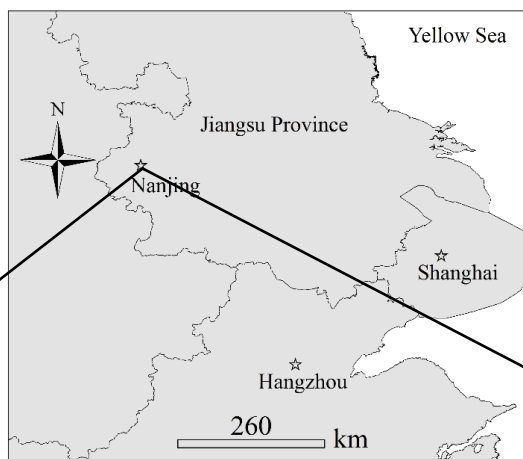
846

847

848

849

850



851





852

853 Fig. 1 Location of the sampling site (the red dot, SS). SP: iron smelt plant; CP: chemical industrial
854 park; RC: residential community. The black line indicates the subway line near SS.

855

856

857

858

859

860

861

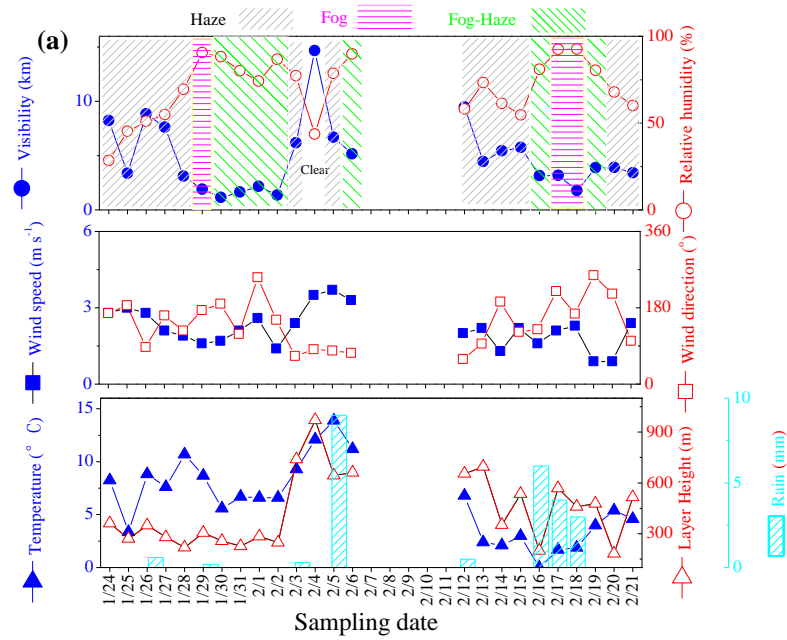
862

863

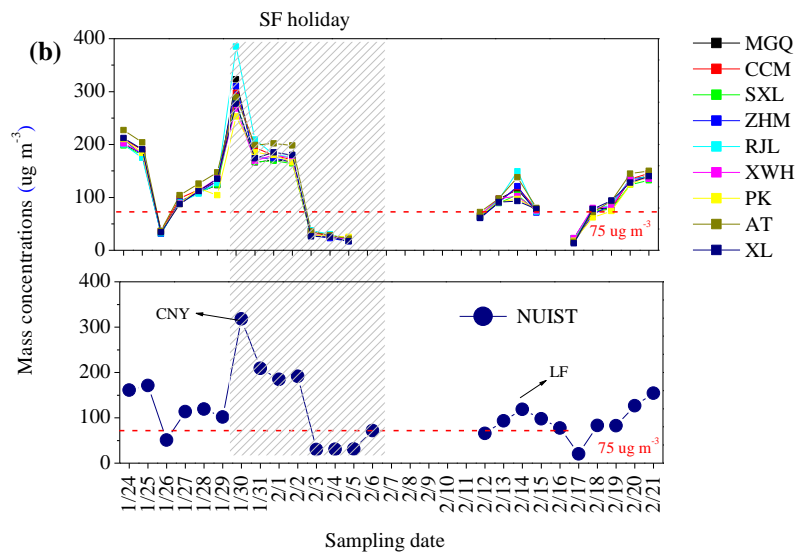
864

865

866



867



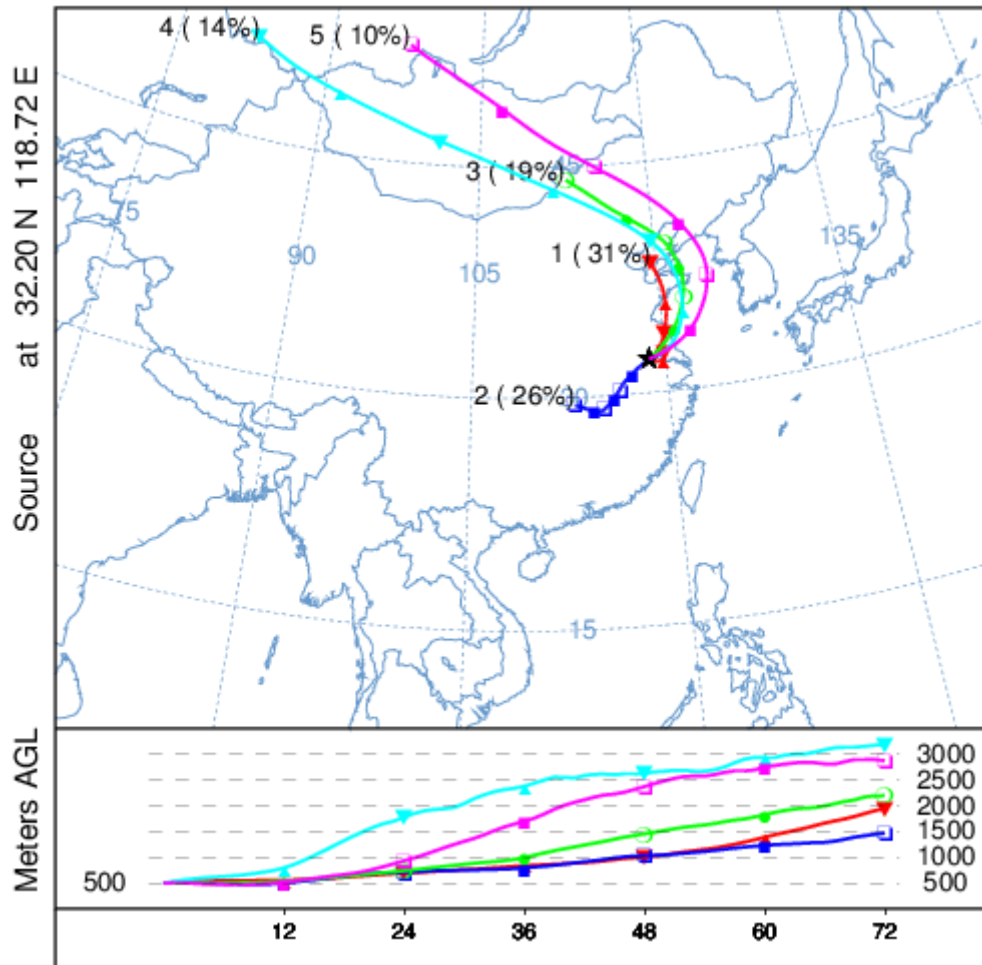
868

869 Fig.2 Daily variation of meteorological factors (a) and mass concentrations of PM_{2.5} (b) during
 870 sampling periods. MGQ, CCM, SXL, ZHM, RJL, XWH, PK, AT and XL indicate the nine urban
 871 air quality monitoring sites set by Jiangsu Environmental Monitoring Center as Supplementary file
 872 S4 shown. NUIST indicates the sampling site of this study at Nanjing University of Information
 873 Science and Technology. SF means Spring Festival (between Jan. 30-Feb.7); CNY means Chinese
 874 New Year day (Jan.30); LF means Lantern Festival day (Feb. 14). 75 $\mu\text{g m}^{-3}$ is the 24 h-averaged
 875 secondary standard value for PM_{2.5} of China National Ambient Air Quality.

876

877

878



879

880 Fig.3 Cluster analysis for backward trajectories of air masses during the whole sampling periods.

881 The different colors indicated different clusters of the backward trajectories.

882

883

884

885

886

887

888

889

890

891

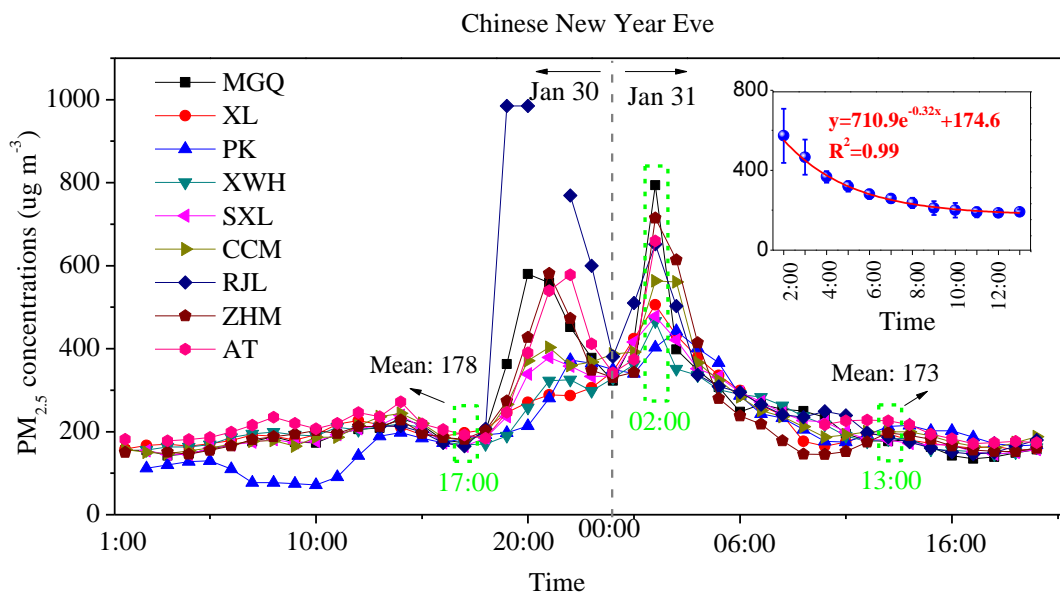
892

893

894

895

896



897

898 Fig.4 Hourly PM_{2.5} concentrations before, during and after Chinese New Year (CNY) Eve of
 899 2014 at Nanjing. The figure at the top-right corner indicates the decreasing trend of averaged
 900 PM_{2.5} mass concentrations after 02:00 of CNY Eve (at Jan. 30, 2014). Hourly data for the nine
 901 sites in urban Nanjing (locations were shown in supplementary file S4) were collected from the
 902 public platform at <http://218.94.78.75/jsair/>.

903

904

905

906

907

908

909

910

911

912

913

914

915

916

917

918

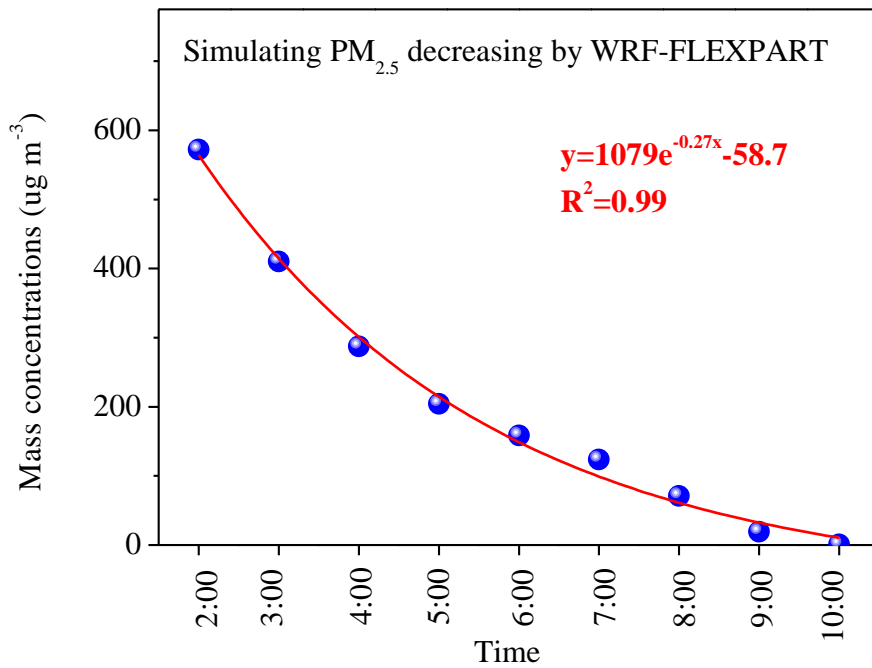
919

920

921

922

923



924

925 Fig.5 Particles decreasing trend at Chinese New Year 's Eve by WRF-FLEXPART simulating. The
 926 particle concentrations decreased to 0.76 $\mu\text{g m}^{-3}$ after nine hours, faster than the real decrease as
 927 Fig.4 shows. It can be explained as that we did not consider the injections of particles during
 928 simulating course, which biases the result.

929

930

931

932

933

934

935

936

937

938

939

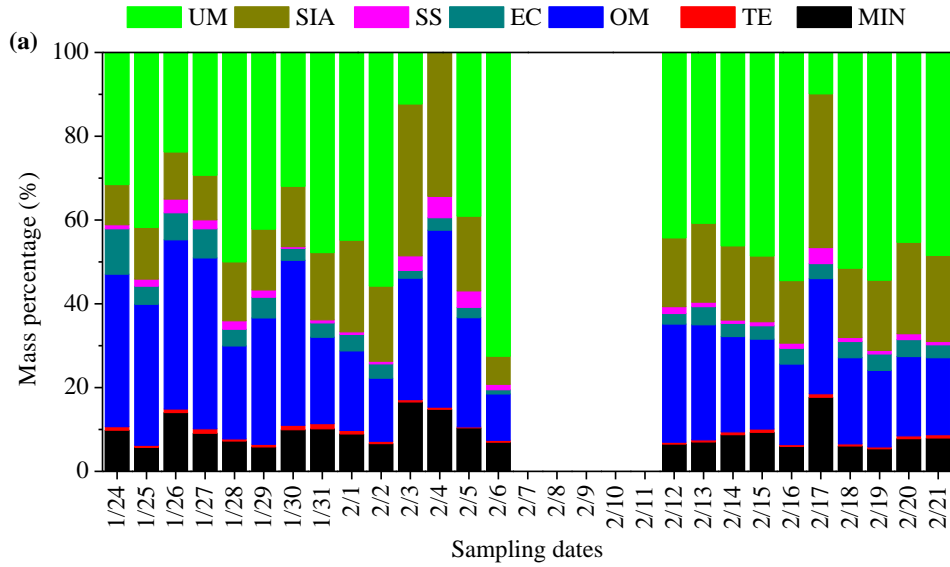
940

941

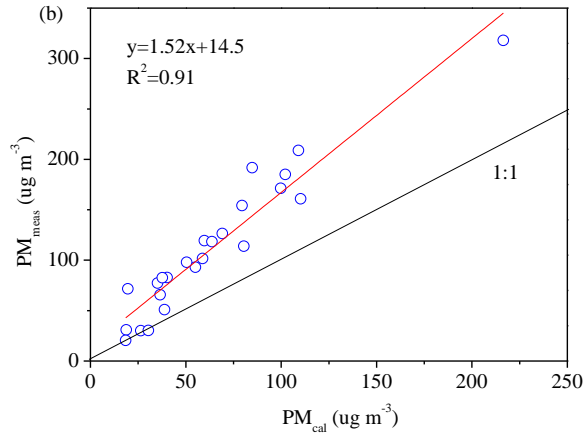
942

943

944



945



946

947 Fig.6 Mass balance of chemical species in $PM_{2.5}$ at sampling periods (a) and relationship between
 948 the mass calculated by adding individual components and the gravimetrically measured particulate
 949 mass (b).

950 $MIN = 2.14 \times Si + 1.67 \times Ti + 1.89 \times Al + 1.59 \times Mn + 1.67 \times Mg + 1.95 \times Ca + 1.35 \times Na + 1.21 \times K + 1.43 \times Fe$.

951 Trace elements (TE) indicated the sum of all other elements except for those used in calculating
 952 MIN. Sea salt (SS) = $[Na^+] + [ss-Cl^-] + [ss-Mg^{2+}] + [ss-K^+] + [ss-Ca^{2+}] + [ss-SO_4^{2-}]$; $ss-Cl^- = 1.8 \times [Na^+]$;
 953 $ss-Mg^{2+} = 0.12 \times [Na^+]$; $ss-K^+ = 0.036 \times [Na^+]$; $ss-Ca^{2+} = 0.038 \times [Na^+]$; $ss-SO_4^{2-} = 0.252 \times [Na^+]$.

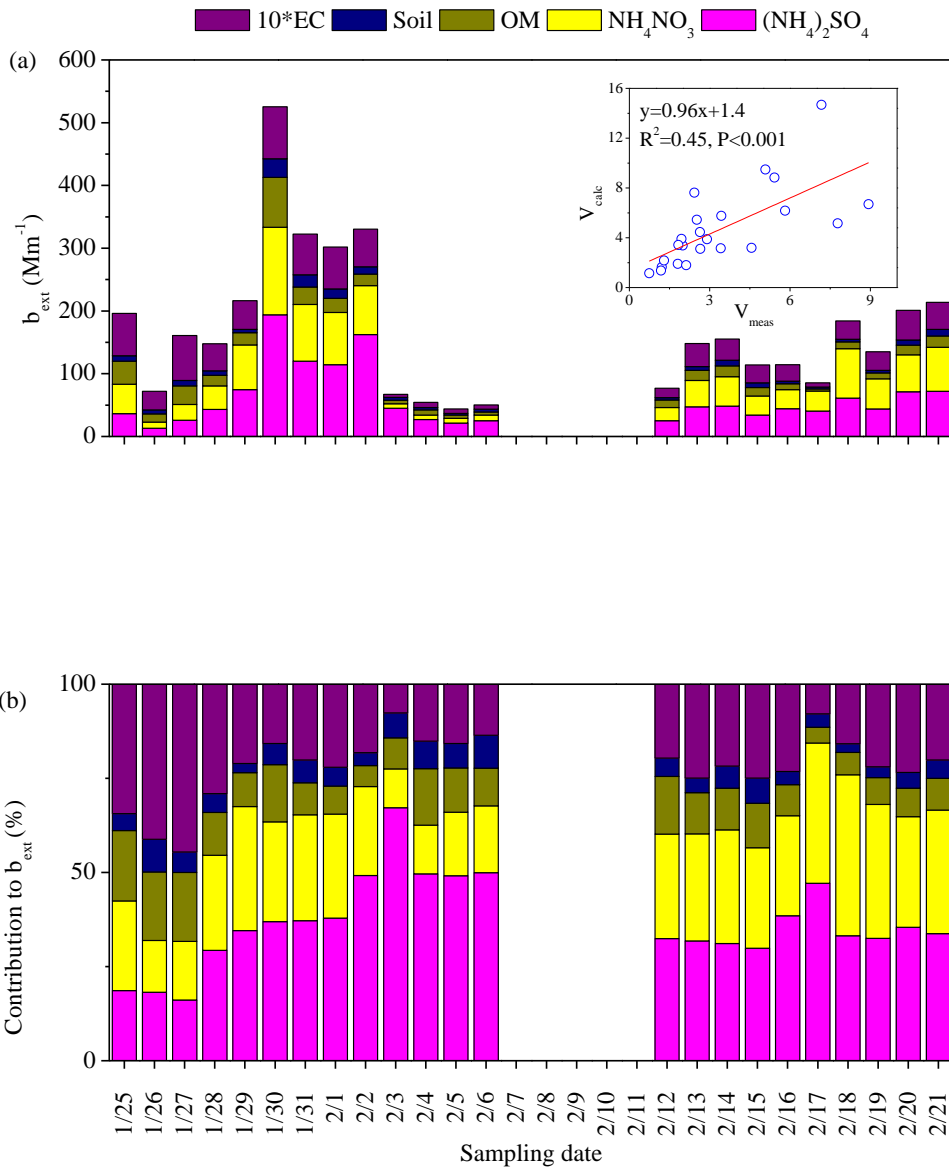
954 Secondary inorganic aerosol (SIA) was calculated as the sum of $nss-SO_4^{2-}$, NO_3^- and NH_4^+ .

955 Organic matter (OM) = $2.0 \times OC$. UM indicated unidentified matter. Jan.30-Feb.7 belongs to the

956 Chinese Spring Festival in 2014; Jan. 30 is the Chinese New Year day; Feb. 14 is the Lantern
 957 Festival day.

958

959



960

961

962 Fig.7 Extinction coefficients of chemical components in $PM_{2.5}$ at Nanjing (a) and relative
 963 contribution to light extinction of chemical components in $PM_{2.5}$ (b). Jan. 30-Feb.7 belongs to the
 964 Chinese Spring Festival in 2014; Jan. 30 is the Chinese New Year day; Feb. 14 is the Lantern
 965 Festival day. V_{calc} indicates the visibility calculated by adding individual components; V_{meas} is the
 966 measured visibility.

967

968

969

970

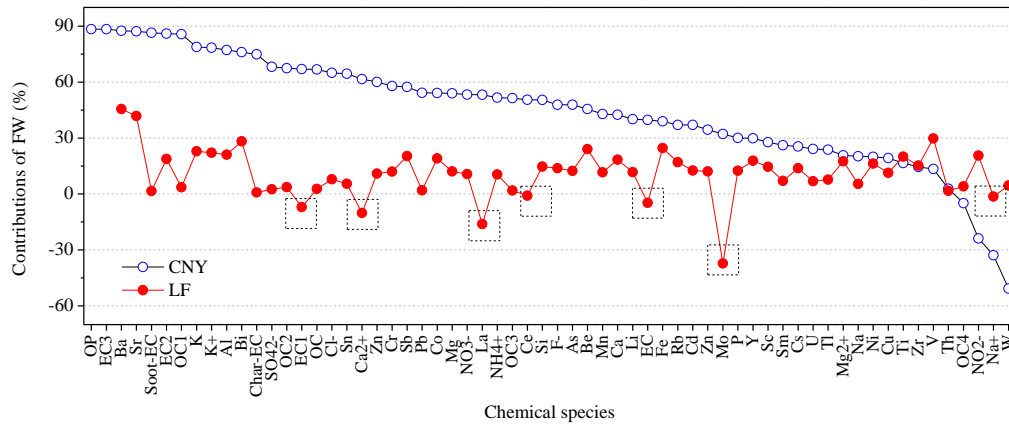
971

972

973

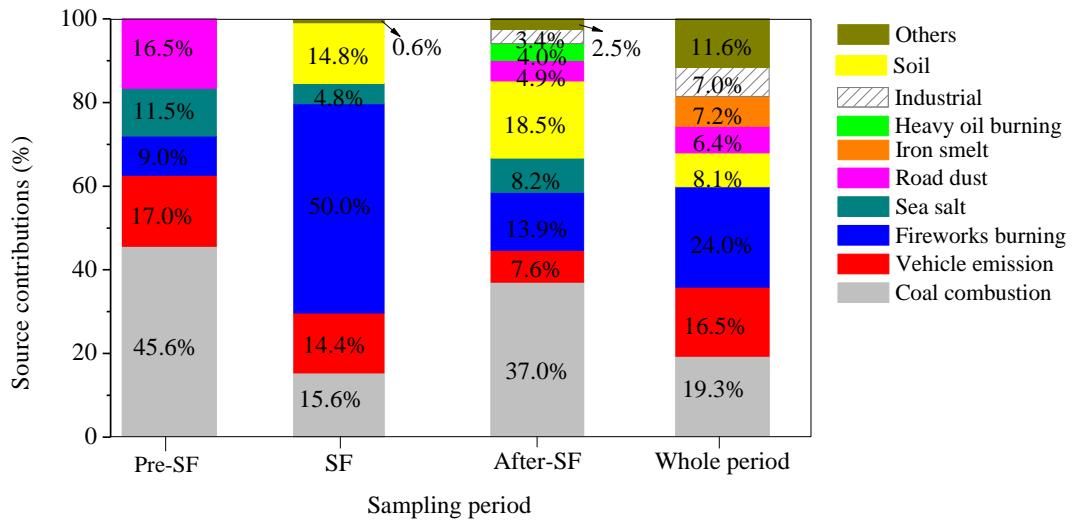
974

975



976
 977
 978
 979
 980
 981
 982
 983
 984
 985
 986
 987
 988
 989
 990
 991
 992
 993
 994
 995
 996
 997
 998
 999

Fig.8 Contributions of fireworks burning (FW) at CNY and LF to chemical species in PM_{2.5}. CNY means Chinese New Year day (Jan. 30); LF means Lantern Festival day (Feb. 14).



1000

1001 Fig.9 Source contributions to atmospheric PM_{2.5} before, during, after 2014 Spring Festival (SF)
 1002 and the whole period by principal component analysis. Pre-SF indicated the period before SF,
 1003 covering the days from Jan. 24 to Jan. 29; SF indicated the period during SF, covering the days
 1004 from Jan. 30 to Feb. 6; After-SF indicated the period after SF, covering the days from Feb.12 to
 1005 Feb.21. **The whole period included Pre-SF, SF and After-SF period.**

1006

1007

1008

1009

1010

1011

1012

1013

1014

1015

1016

1017

1018

1019

1020

1021

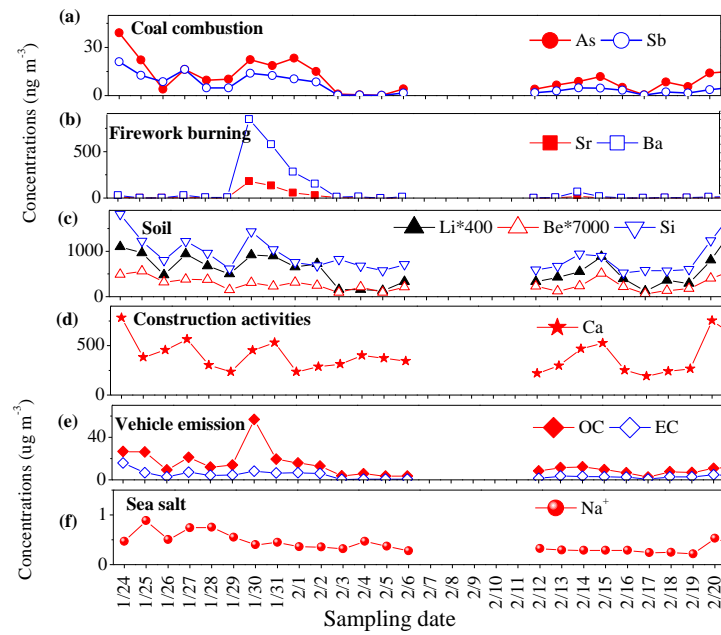
1022

1023

1024

1025

1026



1027

1028 Fig.10 Time series of tracers for (a) coal combustion, (b) fireworks burning, (c) soil, (d)
 1029 construction activities or road dust, (e) vehicle emission and (f) sea salt. The Y-axis units for (a),
 1030 (b), (c) and (d) are ng m^{-3} and are ug m^{-3} for (e) and (f). Jan. 30-Feb.7 belongs to the Chinese
 1031 Spring Festival in 2014; Jan. 30 is the Chinese New Year day; Feb. 14 is the Lantern Festival day.

1032

1033

1034

1035

1036

1037

1038

1039

1040

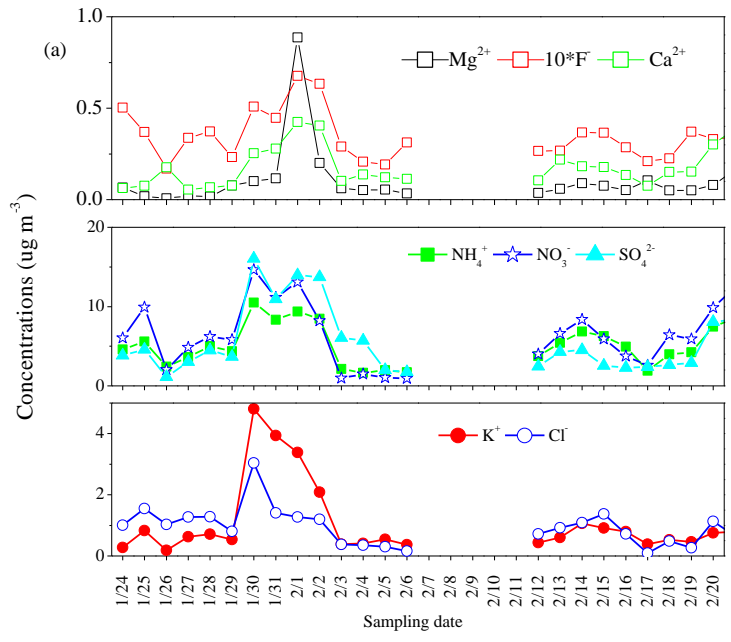
1041

1042

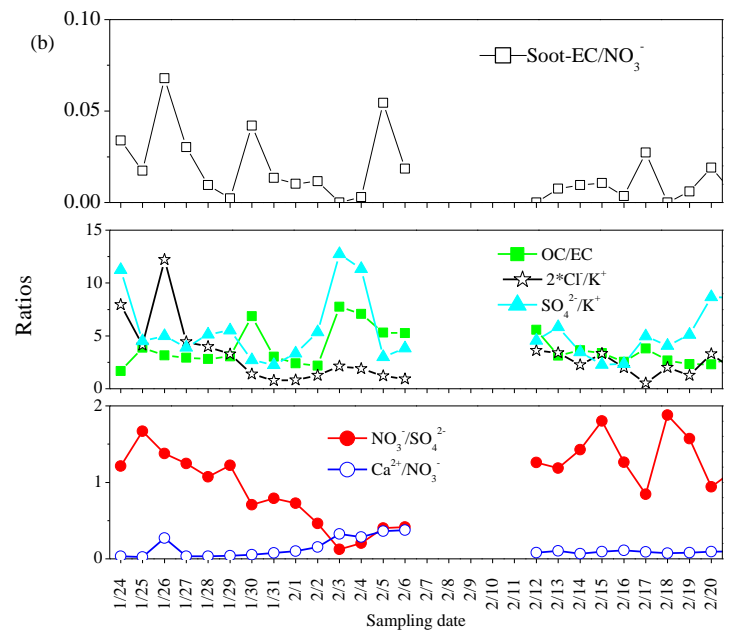
1043

1044

1045



1046



1047

1048 Fig.11 Time series of ions (a) and specific ratios (b) during sampling period. Jan. 30-Feb.7
 1049 belongs to the Chinese Spring Festival in 2014; Jan. 30 is the Chinese New Year day; Feb. 14 is
 1050 the Lantern Festival day.

1051

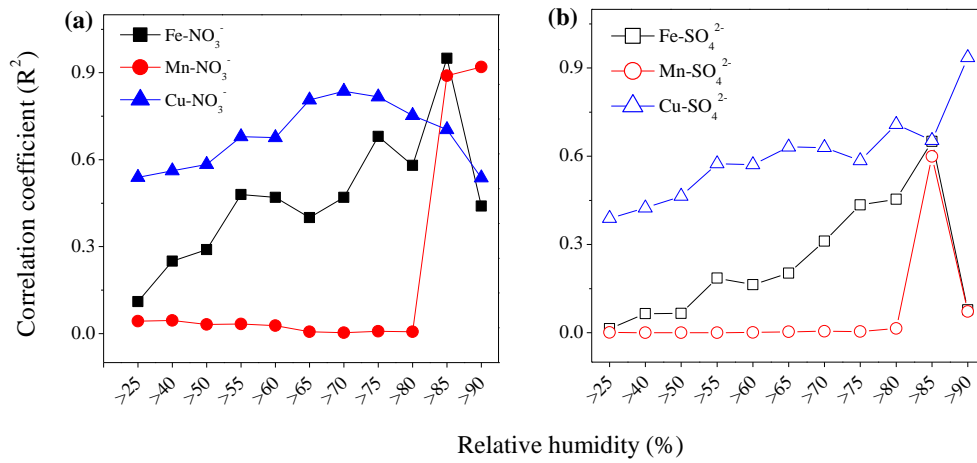
1052

1053

1054

1055

1056



1057

1058 Fig.12 Correlation coefficients (R^2) of NO_3^- and metals-Fe, Mn and Cu under certain relative
 1059 humidity bins (a); correlation coefficients of SO_4^{2-} and metals-Fe, Mn and Cu under certain
 1060 relative humidity bins (b). For each time of calculating the R^2 , the data of NO_3^- or SO_4^{2-} and each
 1061 metal were used for corresponding relative humidity bins.

1062

1063

1064

1065

1066

1067

1068

1069

1070

1071

1072

1073

1074

1075

1076

1077

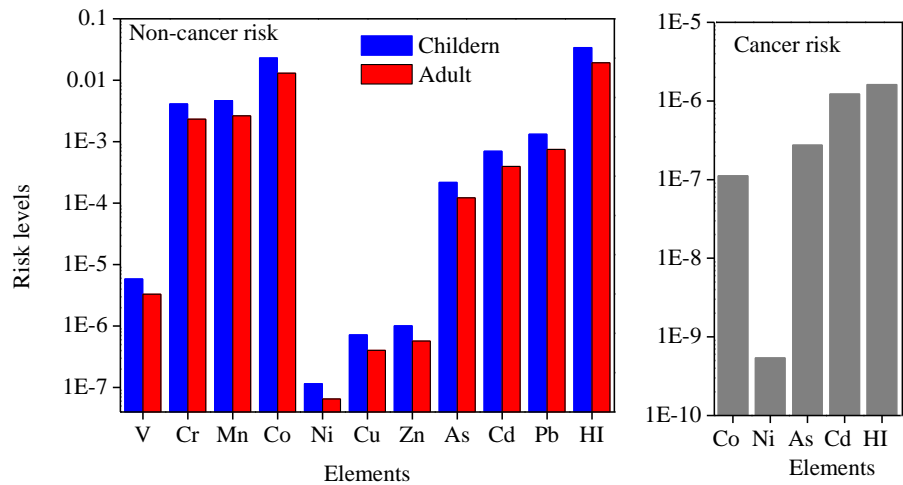
1078

1079

1080

1081

1082



1083

1084 Fig.13 Non-cancer and cancer risks for heavy metals raised by intensive fireworks burning at
 1085 Nanjing.

1086

1087

1088

1089

1090

1091

1092

1093

1094

1095

1096

1097

1098

1099

1100

1101

1102

1103

1104

1105

1106

1107

1108

1109

1110

1111

1112

1113 Table 1 Mass concentrations of elements in PM_{2.5} before, during and after 2014 Chinese Spring Festival at Nanjing (ng m⁻³)

Elements	Pre-SF	SF (without CNY)	After-SF (without LF)	CNY	LF	CNY/pre-CNY	LF/pre-LF
Li	1.9±0.7	1.1±0.8	1.4±1.0	2.3	1.4	1.8	1.3
Be	0.1±0.0	0.0±0.0	0.0±0.0	0.0	0.0	2.1	1.9
Na	826±209	417±196	435±172	563	506	1.3	1.1
Mg	124±79	97±89	106±30	196	124	2.6	1.3
Al	612±234	802±550	530±230	3127	811	7.9	1.7
Si	1105±420	752±147	847±422	1431	943	2.3	1.4
P	66±35	35±20	29±13	42	35	1.5	1.3
K	1940±725	3330±3848	1276±817	14336	2940	9.3	1.8
Ca	454±198	355±95	383±193	454	469	1.9	1.6
Sc	0.1±0.0	0.1±0.0	0.1±0.1	0.1	0.1	1.5	1.4
Ti	31±27	14±8	24±28	20	15	1.2	1.7
V	7.7±2.3	7.0±7.8	6.6±4.6	9.4	10.5	1.2	2.4
Cr	10.4±4.0	7.9±5.7	8.7±3.4	17.4	10.2	2.9	1.3
Mn	48±22	22±19	67±67	47	50	1.9	1.3
Fe	385±342	160±140	261±172	304	300	1.8	1.9
Co	0.4±0.1	0.4±0.4	0.4±0.2	0.6	0.5	2.6	1.6
Ni	8.5±6.0	4.5±3.1	8.9±5.6	5.9	7.6	1.3	1.5
Cu	102±30	81±63	77±25	170	116	1.3	1.3
Zn	257±145	93±81	194±154	242	174	1.6	1.3
As	17±13	9.0±9.8	8.0±4.6	22	8.8	2.2	1.3
Rb	8.5±2.2	4.7±4.2	5.7±4.5	12	6.5	1.7	1.5
Sr	5.1±3.9	34±49	4.9±5.9	181	20.5	79.4	5.7
Y	0.2±0.1	0.1±0.1	0.2±0.1	0.1	0.2	1.5	1.5
Zr	1.9±0.7	1.6±0.6	1.9±1.3	1.6	2.3	1.2	1.4

Mo	2.7±1.0	1.3±1.2	2.9±1.8	2.8	2.7	1.6	0.6
Cd	3.4±2.8	1.3±1.4	1.1±0.7	4.1	1.3	1.7	1.3
Sn	9.0±5.6	5.0±6.1	4.6±3.5	18.0	4.5	3.7	1.1
Sb	11±6.5	4.8±5.4	3.0±1.6	13.9	4.8	2.9	1.7
Cs	1.8±1.0	0.7±0.8	1.4±1.5	1.9	1.2	1.4	1.4
Ba	14±12	152±216	14.4±20.4	850	70.1	99.1	9.7
La	0.7±0.6	0.6±0.5	0.6±0.5	0.6	0.5	2.5	0.8
Ce	0.8±0.5	0.4±0.3	0.6±0.6	0.6	0.5	2.3	1.0
Sm	0.1±0.0	0.0±0.0	0.0±0.0	0.0	0.0	1.4	1.2
W	4.3±2.4	3.1±2.9	3.2±1.3	4.7	5.4	0.6	1.1
Tl	1.4±0.7	0.5±0.5	0.8±0.5	1.4	0.8	1.4	1.2
Pb	187±96	116±132	91±54	425	127	2.6	1.0
Bi	7.3±5.4	9.1±13.0	3.0±2.2	36.9	6.5	7.2	2.3
Th	0.6±0.0	0.5±0.0	0.6±0.0	0.6	0.6	1.0	1.0
U	0.1±0.0	0.0±0.0	0.1±0.1	0.1	0.1	1.4	1.2

1114 Pre-SF indicated the period before 2014 Chinese Spring Festival (SF), covering the days from Jan. 24 to Jan. 29; SF indicated the Spring Festival period, covering
1115 the days from Jan. 30 to Feb.6; After-SF indicated the period after Spring Festival, covering the days from Feb.12 to Feb.21. CNY indicates the Chinese New Year
1116 (CNY) day and in 2014, it is Jan. 30; pre-CNY is the day before CNY and is Jan. 29. LF indicates the Lantern Festival (LF) day and in 2014, it is 14. Feb; pre-LF is
1117 the day before LF and is Feb.14. At CNY and LF, intensive fireworks were burned. Therefore, the mass concentrations of PM_{2.5} and associated chemical species of
1118 the two days were listed separately. CNY/pre-CNY indicates the ratios between mass concentrations of PM_{2.5} and associated chemical species at CNY and the day
1119 before CNY (pre-CNY). LF/pre-LF indicates the ratios between mass concentrations of PM_{2.5} and associated chemical species at LF and the day before LF
1120 (pre-LF).

1121

1122

1123

1124

1125 Table 2 Mass concentrations of ions and carbonaceous species in PM_{2.5} before, during and after 2014 Chinese Spring Festival at Nanjing ($\mu\text{g m}^{-3}$)

Elements	Pre-SF	SF (without CNY)	After-SF (without LF)	CNY	LF	CNY/pre-CNY	LF/pre-LF
Na ⁺	0.65±0.17	0.37±0.07	0.31±0.09	0.40	0.29	0.7	1.0
NH ₄ ⁺	4.26±1.12	4.81±3.68	5.33±1.98	10.5	6.85	2.4	1.3
K ⁺	0.49±0.31	1.59±1.55	0.67±0.22	4.81	1.06	8.9	1.8
Ca ²⁺	0.09±0.05	0.23±0.14	0.19±0.09	0.25	0.18	3.3	0.8
Mg ²⁺	0.03±0.03	0.20±0.31	0.08±0.04	0.10	0.09	1.3	1.5
F ⁻	0.03±0.01	0.04±0.02	0.03±0.01	0.05	0.04	2.2	1.4
Cl ⁻	1.16±0.26	0.72±0.54	0.75±0.40	3.04	1.09	3.8	1.2
NO ₂ ⁻	0.02±0.01	0.04±0.01	0.04±0.01	0.02	0.05	0.8	1.7
NO ₃ ⁻	5.81±2.54	5.27±5.38	6.59±2.98	14.6	8.36	2.5	1.3
SO ₄ ²⁻	3.46±1.28	7.74±5.17	4.05±2.34	16.1	4.54	4.4	1.1
OC	18.2±7.45	9.38±6.70	8.95±3.15	56.9	12.2	4.1	1.1
EC	6.93±4.64	3.12±3.06	2.96±1.20	8.29	3.38	1.8	0.9
OC1	1.87±1.40	0.40±0.23	0.50±0.16	16.1	0.64	33.2	1.1
OC2	4.32±1.65	2.56±1.75	2.36±0.74	14.8	2.86	4.2	1.1
OC3	5.46±2.69	2.77±2.09	2.90±1.15	9.10	4.28	2.4	1.0
OC4	5.44±1.52	3.27±3.03	2.94±1.36	5.81	4.46	0.9	1.1
EC1	7.92±5.07	3.44±2.64	3.15±1.00	18.8	3.30	4.1	0.9
EC2	0.12±0.07	0.07±0.06	0.06±0.05	0.50	0.08	37.7	1.6
EC3	0.00±0.00	0.00±0.00	0.00±0.00	0.11	0.00	-	-
OPC	1.12±2.43	0.39±0.39	0.24±0.43	11.09	0.00	-	-
PM _{2.5}	119.6±43.4	106.9±84.1	88.9±37.4	318.0	118.4	3.1	1.3

1126 - Not detected in the day before CNY and LF.

1127 Pre-SF indicated the period before 2014 Chinese Spring Festival (SF), covering the days from Jan. 24 to Jan. 29; SF indicated the Spring Festival period, covering

1128 the days from Jan. 30 to Feb.6; After-SF indicated the period after Spring Festival, covering the days from Feb.12 to Feb.21. CNY indicates the Chinese New Year

1129 (CNY) day and in 2014, it is Jan. 30; pre-CNY is the day before CNY and is Jan. 29. LF indicates the Lantern Festival (LF) day and in 2014, it is 14. Feb; pre-LF is
1130 the day before LF and is Feb.14. At CNY and LF, intensive fireworks were burned. Therefore, the mass concentrations of $PM_{2.5}$ and associated chemical species of
1131 the two days were listed separately. CNY/pre-CNY indicates the ratios between mass concentrations of $PM_{2.5}$ and associated chemical species at CNY and the day
1132 before CNY (pre-CNY). LF/pre-LF indicates the ratios between mass concentrations of $PM_{2.5}$ and associated chemical species at LF and the day before LF
1133 (pre-LF).